Geostationary Surface Albedo (GSA) Release 2 Validation Report

Doc.No.	:	EUM/OPS/REP/20/1178222
Issue	:	v1D e-signed
Date	:	1 July 2020
WBS/DBS	:	

Change Record

Version	Date	DCR* No. *if applicable*	Description of Changes
1	25/05/2020		Final version for DRR
1D	01/07/2020		Final version for publication, post-DRR

*DCR = Document Change Request

Table of Contents

Table of Figures

Table of Tables

1 INTRODUCTION

Land Surface Albedo products are derived in EUMETSAT by exploiting imagery from geostationary orbit acquired from the Meteosat Visible and Infrared Imager (MVIRI) aboard Meteosat First Generation (MFG) satellites and the Spinning Enhanced Visible and Infrared Imager (SEVIRI) aboard Meteosat Second Generation (MSG) satellites. The Geostationary Surface Albedo (GSA) algorithm developed by EUMETSAT has been used to process the imagery data. This algorithm is an extension of the original Meteosat Surface Albedo (MSA) software developed at the Space Applications Institute of the Joint Research Centre (JRC) of the European Commission. The current release contains improvements and spatial-temporal extensions to that used for Release 1 [AD1]. It provides 10-day composite data of surface albedo estimates derived over the full disk, with maximum extent of 65°N to 65°S and 65°W to 65°E around the nominal Sub-Satellite Point (SSP). The spatial and temporal coverage of the data record is provided in Section 2.3.

1.1 Purpose and Scope

This report contains the validation results for the second release of the Geostationary Surface Albedo (GSA Release 2) Thematical Climate Data Record (TCDR). The retrieval scheme has not been changed since the first release, so the same strengths and weaknesses discussed in [AD1] are present, with the exception of the cloud contamination for which the data record has been improved.

1.2 Applicable Documents

AD1	The Meteosat Surface Albedo Climate Data Record Validation Report (Release 1)	EUM/OPS/REP/13/726421
AD2	Meteosat Surface Albedo Retrieval: Algorithm Theoretical Basis Document	EUM/OPS/SPE/12/3367
AD3	Geostationary Surface Albedo Release 2 Product Users Manual	EUM/CLIMATE/DOC/20/1167370

1.3 Reference Documents

RD1.	C. Schaaf, Z. W. 2015. MCD43A1 MODIS/Terra+Aqua BRDF/Albedo Model Parameters Daily L3 Global - 500m V006. NASA EOSDIS Land Processes DAAC. DOI:10.5067/MODIS/MCD43A1.006
RD2.	Loew, A. and Govaerts, Y.: Towards multidecadal consistent meteosat surface albedo time series, Remote Sens., 2, 957–967. DOI:10.3390/rs2040957, 2010.
RD3.	Y. M. Govaerts, B. Pinty, M. Taberner, A. Lattanzio, "Spectral conversion of surface albedo derived from meteosat first generation observations", IEEE Geosci. Remote Sens. Lett., vol. 3, pp. 23-27, Jan. 2006.
RD4.	Wang, Z., Schaaf, C., Lattanzio, A., Carrer, D., Grant, I., Román, M., Camacho, F., Yu, Y., Sánchez-Zapero, J. & Nickeson, J. (2019). Global Surface Albedo Product Validation Best Practices Protocol. Version 1.0. In Z. Wang, J. Nickeson & M. Román (Eds.), Best Practice for Satellite Derived Land Product Validation (p. 45): Land Product Validation Subgroup (WGCV/CEOS). DOI:10.5067/DOC/CEOSWGCV/LPV/ALBEDO.001
RD5.	GCOS-92 (2004), Implementation Plan For The Global Observing System For Climate In Support Of The UNFCCC.
RD6.	Algorithm Theoretical Basis Document Meteosat Cloud Fractional Cover (COMET) Edition 1, 2017. DOI: 10.5676/EUM SAF CM/CFC METEOSAT/V001

RD7.	Lewis, P., and M. Barnsley (1994), Influence of the sky radiance distribution on various formulations of the earth surface albedo, Proc. Conf. Phys. Meas. Signatures Remote Sens., 707–715
RD8.	Pinty, B., A. Lattanzio, J. V. Martonchik, M. M. Verstraete, N. Gobron, M. Taberner, J.-L. Widlowski, R. E. Dickinson, and Y. Govaerts (2005), Coupling Diffuse Sky Radiation and Surface Albedo, J. Atmos. Sci.. DOI:10.1175/JAS3479.1.
RD9.	Pinty, B., F. Roveda, M. M. Verstraete, N. Gobron, Y. Govaerts, J. V. Martonchik, D. J. Diner, and R. A. Kahn, 2000a: Surface albedo retrieval from Meteosat 1. Theory. J. Geophys. Res., 105(D14), 18 099–18 112.
RD10.	Pinty, B., F. Roveda, M. M. Verstraete, N. Gobron, Y. Govaerts, J. V. Martonchik, D. J. Diner, and R. A. Kahn, 2000b: Surface albedo retrieval from Meteosat 2. Applications. J. Geophys. Res., 105(D14), 18 113–18 134.
RD11.	Lattanzio, A., Y. Govaerts, and B. Pinty (2006), Consistency of surface anisotropy characterization with Meteosat observations, Adv. Space Res., 39(1), 131–135. DOI:10.1016/j.asr.2006.02.049
RD12.	Govaerts, Y., and A. Lattanzio (2007), Retrieval error estimation of surface albedo derived from geostationary large band satellite observations: Application to Meteosat-2 and -7 data, J. Geophys. Res., 112, D05102. DOI:10.1029/2006JD007313
RD13.	Lattanzio, A.; Schulz, J.; Matthews, J.; Okuyama, A.; Theodore, B.; Bates, J.J.; Knapp, K.R.; Kosaka, Y.; Schüller, L. Land Surface Albedo from Geostationary Satelites: A Multiagency Collaboration within SCOPE-CM. Bull. Amer. Meteorol. Soc 2013, 94, 205–214. DOI: 10.1175/BAMS-D-11-00230.1
RD14.	Loew, A., Bennartz, R., Fell, F., Lattanzio, A., Doutriaux-Boucher, M., and Schulz, J.: A database of global reference sites to support validation of satellite surface albedo datasets (SAVS 1.0), Earth Syst. Sci. Data, 8, 425-438. DOI:10.5194/essd-8-425-2016
RD15.	Schaaf C. , Z. W. 2015. MCD43A1 MODIS/Terra+Aqua BRDF/Albedo Model Parameters Daily L3 Global - 500m V006. NASA EOSDIS Land Processes DAAC. DOI: 10.5067/MODIS/MCD43A1.006
RD16.	Privette J. L., M. Mukelabai, N. Hanan, and Z. Hao. 2005. SAFARI 2000 Surface Albedo and Radiation Fluxes at Mongu and Skukuza, 2000-2002.Data set. Available on-line [http://daac.ornl.gov/] from Oak Ridge National Laboratory Distributed Active Archive Center, Oak Ridge,\\ Tennessee, U.S.A. doi:10.3334/ORNLDAAC/786.
RD17.	Lattanzio, A., Fell, F., Bennartz, R., Trigo, I. F., and Schulz, J.: Quality assessment and improvement of the EUMETSAT Meteosat Surface Albedo Climate Data Record, Atmos. Meas. Tech., 8, 4561–4571. DOI: 10.5194/amt-8-4561-2015, 2015
RD18.	Dee et al., The ERA-Interim reanalysis: configuration and performance of the data assimilation system, https://doi.org/10.1002/qj.828, QJRMet, 2011.
RD19.	Govaerts, Y. M., Lattanzio, A., Taberner, M. and Pinty, B.: Generating global surface albedo products from multiple geostationary satellites, Remote Sensing of Environment, 112(6), 2804–2816, doi:10.1016/j.rse.2008.01.012, 2008.
RD20.	Iglewicz B. and Hoaglin D. (1993), "Volume 16: How to Detect and Handle Outliers", The ASQC Basic References in Quality Control: Statistical Techniques, Edward F. Mykytka, Ph.D., Editor.

1.4 Acronyms

AD	Applicable Document
AOT	Aerosol Optical Thickness
ATBD	Algorithm Theoretical Basis Document
BHR	Bi-Hemispherical Reflectance
BHRiso	BHR under perfect isotropic illumination conditions (or WSA)
BRDF	Bidirectional Reflectance Distribution Function
BSA	Black Sky Albedo (or DHR)
CFC	Cloud Fractional Cover
CLM	CLoud Mask
CSDP	Climate Service Development Plan
DHR	Directional Hemispherical Reflectance (or BSA)
DHR30	DHR estimated with the sun zenith angle fixed at 30 degrees
ECMWF	European Centre for Medium-Range Weather Forecasts
EUMETSAT	European Organisation for the Exploitation of Meteorological Satellites
GCOS	Global Climate Observing System
GSA	Geostationary Surface Albedo
HRV	High Resolution Visible
INDOEX	INDian Ocean EXperiment
IODC	Indian Ocean Data Coverage
ITCZ	Intertropical Convergence Zone
JRC	Joint Research Centre
LUT	Look-Up Table
MAE	Mean Absolute Error
MFG	Meteosat First Generation
MODIS	Moderate Resolution Imaging Spectroradiometer
MSA	Meteosat Surface Albedo
MSG	Meteosat Second Generation
MVIRI	Meteosat Visible and Infrared Imager
NWP	Numerical Weather Prediction
ORNL DAAC	Oak Ridge National Laboratory Distributed Active Archive Center
PERC	PERCentage
RMSE	Root Mean Square Error
RPV	Rahman–Pinty–Verstraete
RTM	Radiative Transfer Model
SAF	Satellite Application Facility
SAFARI	Southern African Regional Science Initiative
SEVIRI	Spinning Enhanced Visible and Infrared Imager
SSP	Sub-Satellite Point

SSR	Sensor Spectral Response
TCDR	Thematical Climate Data Record
TCO3	Total Column Ozone
TCWV	Total Column Water Vapour
VIS	VISible
VR	Validation Report
WSA	White Sky Albedo (or BHRiso)

1.5 Definitions

The following definitions, from [RD4], clarify the physical meaning of the different variables, measurable from satellite observations, describing the land surface albedo.

- **Black-Sky Albedo (BSA) or Directional Hemispherical Reflectance (DHR):** is the albedo in the absence of any diffuse irradiance component (no atmospheric scattering), with only a direct illumination component. The Global Climate Observing System (GCOS) implementation plan [RD5] specifies that the black-sky albedo is the product required for climate change purposes.

- **White-Sky Albedo (WSA) or bi-hemispherical albedo under isotropic illumination (BHR$_{iso}$):** is the albedo in the absence of any direct illumination component but only comprised of isotropic diffuse illumination. This component is sensitive to the intrinsic coupling between the surface and the scattering atmosphere.

- **Blue-Sky Albedo:** Blue-sky albedo comprises both direct and diffuse components and represents the albedo of the surface with respect to specific atmospheric conditions. A simple form of blue-sky albedo can be calculated with an assumption of isotopically diffuse radiation and can be expressed as a linear combination of DHR and BHRiso ([RD7] and [RD8]).

2   DATA RECORD SUMMARY

A complete and detailed mathematical description is provided in the Algorithm Theoretical Basis Document (ATBD) [AD2]. The algorithm is based on a method proposed by Pinty et al. ([RD9] and [RD10]) to retrieve the surface anisotropy and the atmospheric aerosol load through the inversion of a Radiative Transfer Model (RTM), through the accumulation of geostationary cloud-free observations acquired in the visible part of the electromagnetic spectrum at different illumination conditions (see Figure 1). This retrieval scheme relies on the applicability of the reciprocity principle at a spatial scale of several kilometres [RD11]. According to this principle, measurements taken at different viewing angles correspond to similar measurements in different sun illumination conditions. The usage of Meteosat data only cannot guarantee a robust and accurate retrieval. In order to limit the retrieval to the surface–aerosol system only, the atmospheric state is further characterized by the ingestion of Total Column Ozone (TCO3) and Total Column Water Vapour (TCWV) from the reanalysis (ERA-interim) at the European Centre for Medium-Range Weather Forecasts (ECMWF).
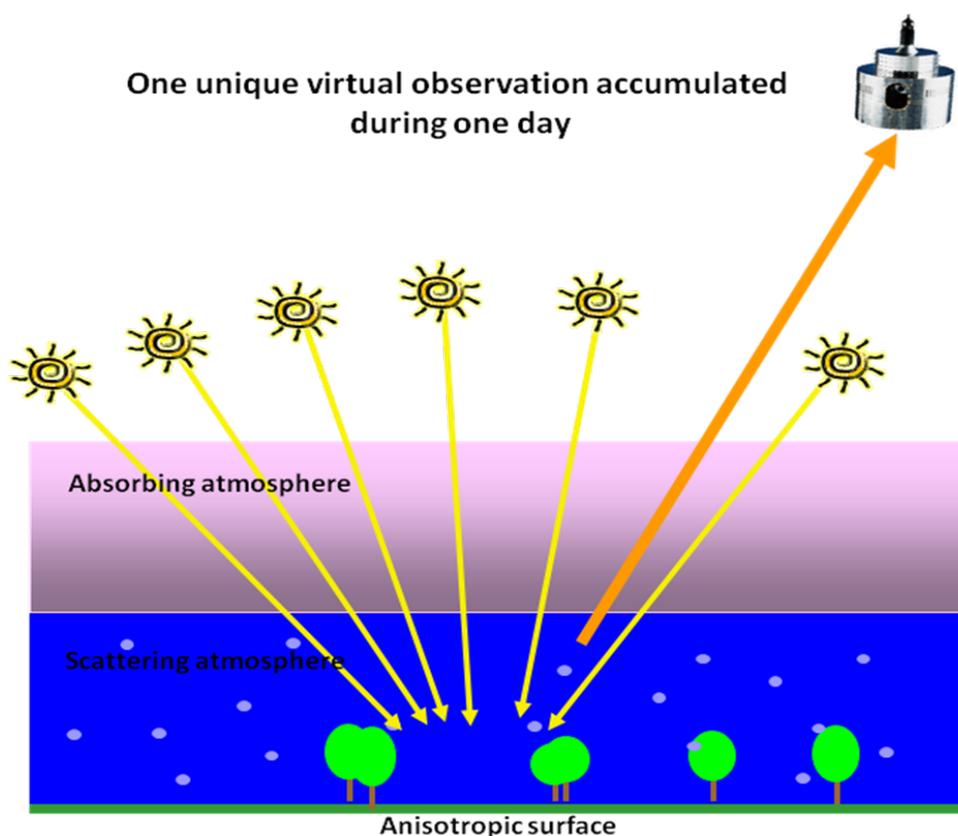
Figure 1: GSA Retrieval scheme. The observations accumulated during the day are used as an angular sampling of the surface.

Due to the large-scale calculations needed, in particular for the generation of a decades-long data record, the number of possible states of the coupled surface-aerosol system are limited to a fixed number. The usage of pre-calculated Look-Up Tables (LUTs) speeds up the per pixel base retrieval. The algorithm also estimates retrieval uncertainty and provides a probability for the retrieval [RD12], calculated according to the quality of the fit and the actual number of available observations.

The retrieval is performed using the spectral instrument visible channel for MVIRI (Meteosat-2 to Meteosat-7) and in the High-Resolution Visible (HRV) channel for SEVIRI (Meteosat-8 to Meteosat-10). The product contains also the uncertainties and other ancillary information. Figure 2 shows the spectral bands for the individual instruments giving an indication how diverse they are. In the retrieval process, it is assumed that the SSR do not change in time and are not affected by any uncertainty. In order to make the albedo estimates comparable and enable comparison with other surface albedo data records, e.g. the MODIS data record used as a reference, the albedo quantities retrieved with GSA needed to be converted into a broadband spectral interval (0.3-3.0 μm). This conversion to broadband is done for MVIRI following the outcome in [RD2] and for SEVIRI following the method in [RD3]. The complete list of coefficients for calculating broadband albedo estimates from the spectral retrieved quantities can be found in [AD3].
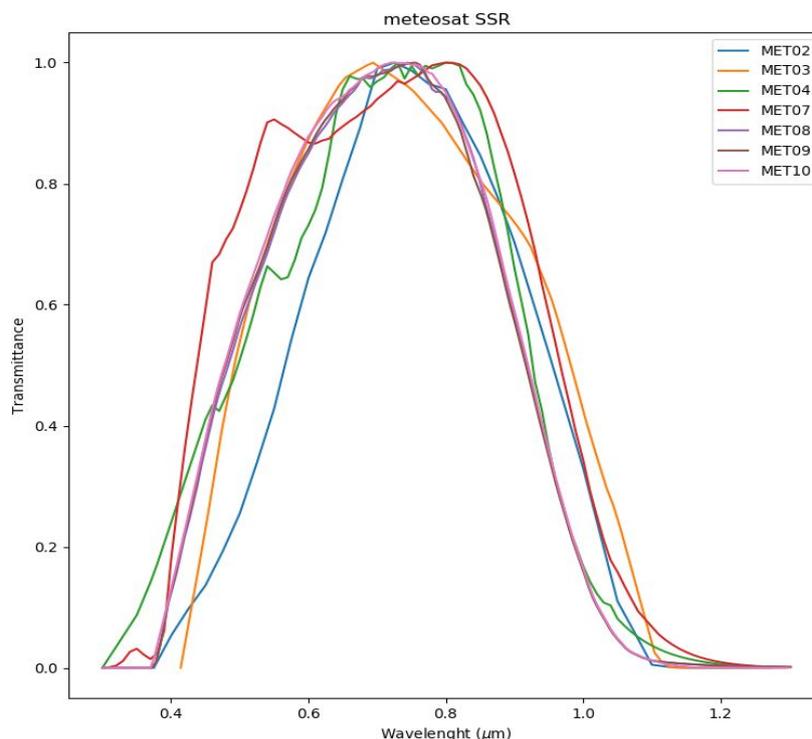
Figure 2: Sensor Spectral Response (SSR) for the VIS (HRV) band of MVIRI (SEVIRI)

2.1 Input Data

The input data for the GSA algorithm are divided into two classes: dynamic (see Table 1) and static (see Table 2). In the class of the dynamic inputs are Meteosat imagery cloud mask and reanalysis data. Static input data are look-up tables for the model inversion and the latitude/longitude information.

2.1.1 Meteosat Imagery

This release contains products generated with imagery acquired by both MVIRI and SEVIRI instruments. MVIRI is the Meteosat Visible Infra-Red Imager instrument that was operated on-board EUMETSAT's Meteosat First Generation (MFG) series of European geostationary satellites during the years 1977 – 2017. The MFG series consisted of seven satellites. The first MFG satellite (Meteosat-1) was launched in 1977 but failed in late 1979. Meteosat-2 became operational

in late 1982 and since then an unbroken data record exists. This TCDR, however, includes data only from Meteosat-5 located at 63°E and Meteosat-7 located at 57°E.

File	Meaning	Units
Radiance	Radiance at pixel resolution in the instrument visible band	$Wm^{-2}\ sr^{-1}$
Cloud Mask	Cloud mask at pixel level. If not present, the algorithm assumes all pixels are cloud-free. 0: Cloud free (CFC=0) 1: Cloudy (CFC != 0)	1
Model Reanalysis Data (ERA-interim)	Total Column Ozone (TCO3) and Total Column Water Vapour (TCWV). If the values are not provided, default values are used : TCO3 : 0.3 cm.atm TCWV : 2.0 g/cm^2	TCO3: cm atm TCWV: g/cm^2

Table 1: GSA dynamic input files

File	Meaning
Look Up Table (LUT)	Binary files. The LUTs contains pre-computed integrals used for the RTM inversion
Latitude	Latitude of the MVIRI/SEVIRI rectified images
Longitude	Longitude of the MVIRI/SEVIRI rectified images

Table 2: Ancillary files GSA static input

SEVIRI is the Spinning Enhanced Visible and Infra-Red Imager instrument which has been flown on EUMETSAT's Meteosat Second Generation (MSG) satellites. The MSG series consists of four satellites, the first of which (Meteosat-8) was launched in August 2002. This release contains products generated at 0° for Meteosat-8, 9, 10 (Figure 3).

All Meteosat positions over the Indian Ocean, irrespective of the satellite generation, are part of the so-called IODC data service established to support the international Indian Ocean Experiment (INDOEX) in 1998. Meteosat-5 was moved to a position at 63°E and started its operational service on 1 July 1998. Due to its scientific relevance, the service was continued with Meteosat-7 at 57°E from December 2006 onwards.
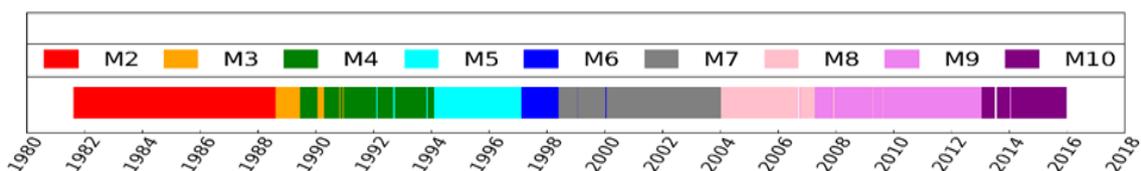

Figure 3: Operational Meteosat prime satellite over the period.

2.1.2   Cloud Mask

The cloud mask is generated for both MVIRI and SEVIRI using the same algorithm developed by MeteoSwiss, at the EUMETSAT Climate Monitoring SAF [RD6]. This algorithm has been chosen because it is applicable for the imagers on board both first and second generations of Meteosat satellites. The implemented scheme is based on a Bayesian approach applied to a set of scores calculated by exploiting only the two visible SEVIRI channels (or the one single visible channel for MVIRI) and the thermal IR channel around 10.8 µm. The algorithm also builds up a daily background reflectance map to assess potential clouds with higher reliability. The mask is provided for each image pixel as a Cloud Fractional Cover (CFC) in eight steps from zero to 100%. Only pixels with CFC=0 are considered for processing.

2.1.3   Reanalysis Data

Several ozone and water vapour absorption bands are located within the Meteosat visible channel and the effects of these gases on radiation transfer processes need to be considered. Total Column Ozone (TCO3) and Total Column Water Vapour (TCWV) estimates from the ECMWF ERA-interim reanalysis [RD18] are used (Table 1) in one of the Look-Up Tables (LUT) to invert the Rahman–Pinty–Verstraete (RPV) Radiative Transfer Model (RTM) (see [AD2]), used as the forward model in GSA. The sensitivity of the retrieval scheme with respect to these atmospheric parameters has been analysed in [AD2].

2.2   Data Processing Strategy

The processing consists of three steps shown in this figure:
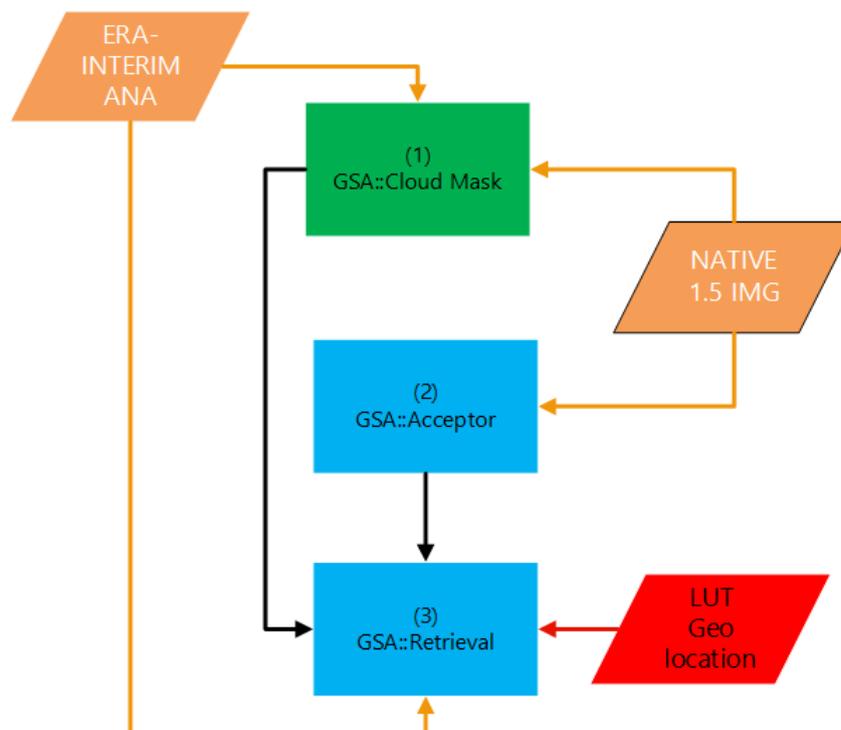
Figure 4: GSA processing steps.

(1) <u>GSA::Cloud Mask</u>: The Cloud Mask is generated for both MVIRI and SEVIRI using the algorithm developed by MeteoSwiss at the Climate Monitoring SAF [RD6]. The implemented scheme is based on a Bayesian approach applied to a set of scores calculated

exploiting only the two visible SEVIRI channels (one single visible channel for MVIRI) and the thermal IR channel around 10.8 μm. The algorithm also builds up a daily background reflectance map to assess potential clouds with higher reliability. The mask is provided as a Cloud Fractional Cover (CFC) in 8 steps from 0 to 100%. Only pixels with a CFC=0 are used because considered as cloud free.

(2) <u>GSA::Acceptor:</u> The native input Level 1.5 Meteosat images in the native instrument-specific format are converted into a unique format, valid for any instrument. Information about calibration, radiometric quality and aspects are also included in this format.

(3) <u>GSA::Retrieval:</u> Generate 10-day albedo records as described in [AD2].

2.3   Spatial and Temporal Coverage

The temporal coverage (see Table 3) of the data record is about 36 years for the prime mission at 0° longitude (see Figure 3). For the IODC mission the temporal coverage is about 19 years. Of course, some gaps are present, due to missing images. It is important to highlight that for each pixel, a minimum of six daylight and cloud free measurements for each day are necessary to retrieve the albedo variables. If this threshold is not reached, no retrieval is performed. Periods when the prime satellite changes from one platform to another and then back, will also contain gaps, because GSA cannot process together images acquired by different platforms in the same 10-day period. A comprehensive view of the gaps can be found in Appendix A.

Satellite	*Instrument/Channel*	*Mission (SSP)*	*Start Date*	*End Date*
Meteosat-2	MVIRI/VIS	0DEG (0°)	1981-08-16	1988-08-11
Meteosat-3	MVIRI/VIS	0DEG (0°)	1988-08-11	1991-01-25
Meteosat-4	MVIRI/VIS	0DEG (0°)	1989-06-19	1994-02-04
Meteosat-5	MVIRI/VIS	0DEG (0°)	1991-05-02	1997-02-13
		IODC (63°E)	1998-07-01	2007-04-16
Meteosat-6	MVIRI/VIS	0DEG (0°)	1996-10-21	2000-01-20
Meteosat-7	MVIRI/VIS	0DEG (0°)	1998-06-03	2006-07-19
		IODC (57°E)	2006-11-01	2017-03-31
Meteosat-8	SEVIRI/HRV	0DEG (0°)	2004-03-01	2007-05-31
Meteosat-9	SEVIRI/HRV	0DEG (0°)	2007-05-01	2013-04-30
Meteosat-10	SEVIRI/HRV	0DEG (0°)	2013-04-01	2017-12-31

Table 3: Satellite, instrument, mission, nominal orbit position and services for the period 1981-2017. The period includes Meteosat 2-7 (MFG) and Meteosat 8-10 (MSG).
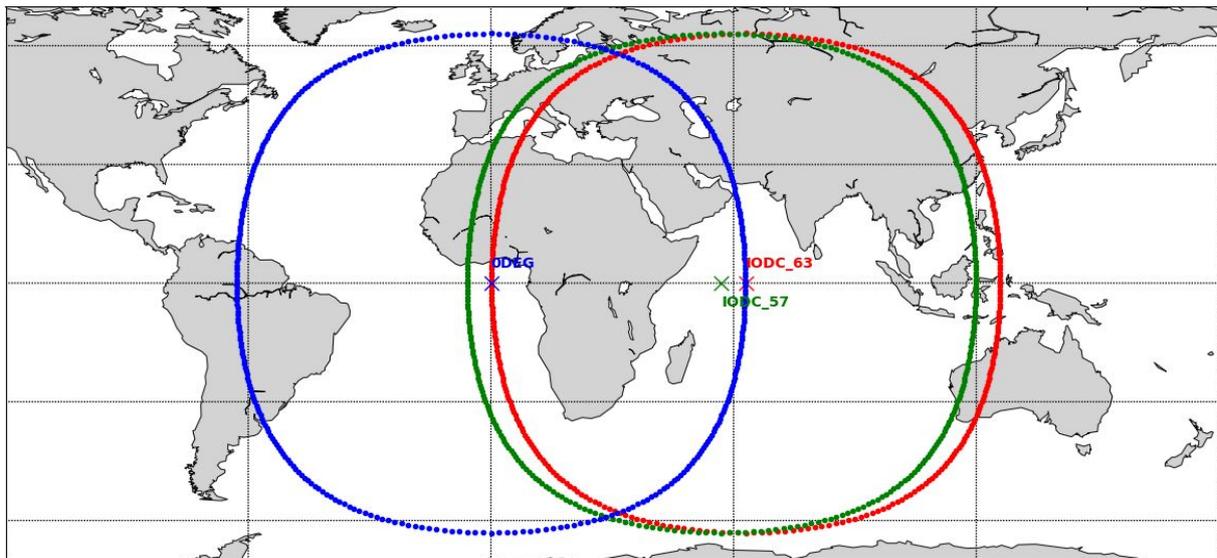
Figure 5: 0DEG (in blue), IODC (57E in green and 63E in red) spatial coverage.

3 VALIDATION DATA

3.1 Validation sites

The validation sites used are ones selected from the list of Surface Albedo Validation Sites (SAVS)[1] listed in [RD14]. The following locations have been used for validation with the reference data described in Section 3.2. The particular locations were chosen to cover different parts of the disk and the most common surface types.

SITE NAME	LAT	LON	SURFACE TYPE
LIBIA_00001	27.4742	16.276	Bare soil
EGYPT_ONE	27.12	26.1	Bare soil
MORZUQ_DESERT	12.5	24.75	Bare soil
SOV	24.91	46.41	Bare soil
MONGU	-15.2536	23.1508	Urban
SKUKUZA	-25.02	31.4834	Shrubland
BELMANIP_00027	-11.0438	-39.9664	Vegetation

Table 4: SAVS sites used for comparison with reference data. Latitude and Longitude are given in decimal degrees.

A comparison against in-situ measurements was made for the MONGU and SKUKUZA sites. For the remaining locations, the comparison against another satellite product (see following Section 3.2) was made.

3.2 Reference data

The following data records have been used as references in the comparison with the GSA data record.

- MODIS: The Moderate Resolution Imaging Spectroradiometer V006 MCD43A1 product containing daily L3 albedo values and BRDF parameters at 500m resolution [RD15]. The data have been downloaded from the ORNL DAAC Oak Ridge National Laboratory

---

[1] DOI: http://dx.doi.org/10.15770/EUM_SEC_CLM_1001

Distributed Active Archive Center with their global subset tool. Shortwave (0.3-5.0µm) DHR30 is calculated from the BRDF parameters following the formula provided by the MODIS team[2].

- SAFARI: Top-of-the-canopy broadband Blue Sky Albedo (see Section 1.5) and radiation fluxes are calculated from measurements performed at flux towers on sites in southern Africa from a campaign conducted from March 2000 through December 2002 [RD16].

One has to note that the quantity compared are not the same, BHR (blue-sky albedo) for SAFARI and DHR30 (black-sky albedo) for GSA and MODIS. The BHR contains the diffuse component of albedo, missing for the DHR30, only containing the direct one. The diffuse component is strongly dependent on the aerosol content, expected to be relevant over an urban site such as MONGU. However, this comparison provides an qualitative indication of the goodness of the retrieval.

4   QUALITY EVALUATION

4.1   Comparison with Meteosat Surface Albedo Release 1

Release 1 is referred to Meteosat Surface Albedo (MSA), while Release 2 to Geostationary Surface Albedo (GSA). The retrieval core is the same but GSA has an extra processing layer allowing the application to any Geostationary satellite [RD13], while MSA only allowed the processing of Meteosat First Generation imagery.

GSA Release 2, compared to Release 1, is significantly longer by making the GSA retrieval applicable to Meteosat Second Generation data and the extension of the product spatial coverage that includes now the part of South America covered by the Meteosat 0° longitude mission.

The main improvement of GSA Release 2 compared to Release 1 is the exploitation of an external cloud mask. The residual cloud contamination is the most relevant factor affecting the quality of Release 1 [AD1]. In order to verify that the cloud contamination in this release has decreased, two regions have been analysed. The precipitation regime in these regions (and the cloud coverage) is known to depend on the shift of the Intertropical Convergence Zone (ITCZ) and the African Monsoon[3]. More precipitation is expected north of the Equator from June to September, and south of the Equator from January to March (see Figure 6). Because the level of precipitation is related to the amount of cloud and its temporal persistence, the impact of using or not using an external cloud mask should show a clear signature. In order to check the presence of such a signature, the Release 1 and Release 2 DHR30 values retrieved over two regions; one north and one south of the Equator, have been compared for the year 2001. The plots in Figure 7 and Figure 9 show the average DHR30 over the region for each 10-day period in the year and the standard deviation is represented as the error bar.

---

[2] Link valid 30/03/2020: https://www.umb.edu/spectralmass/terra_aqua_modis/v006

[3] Source: Climate and Ocean: Variability, Predictability and Change (CLIVAR) http://www.clivar.org/african-monsoon (Link valid 15/03/2020)
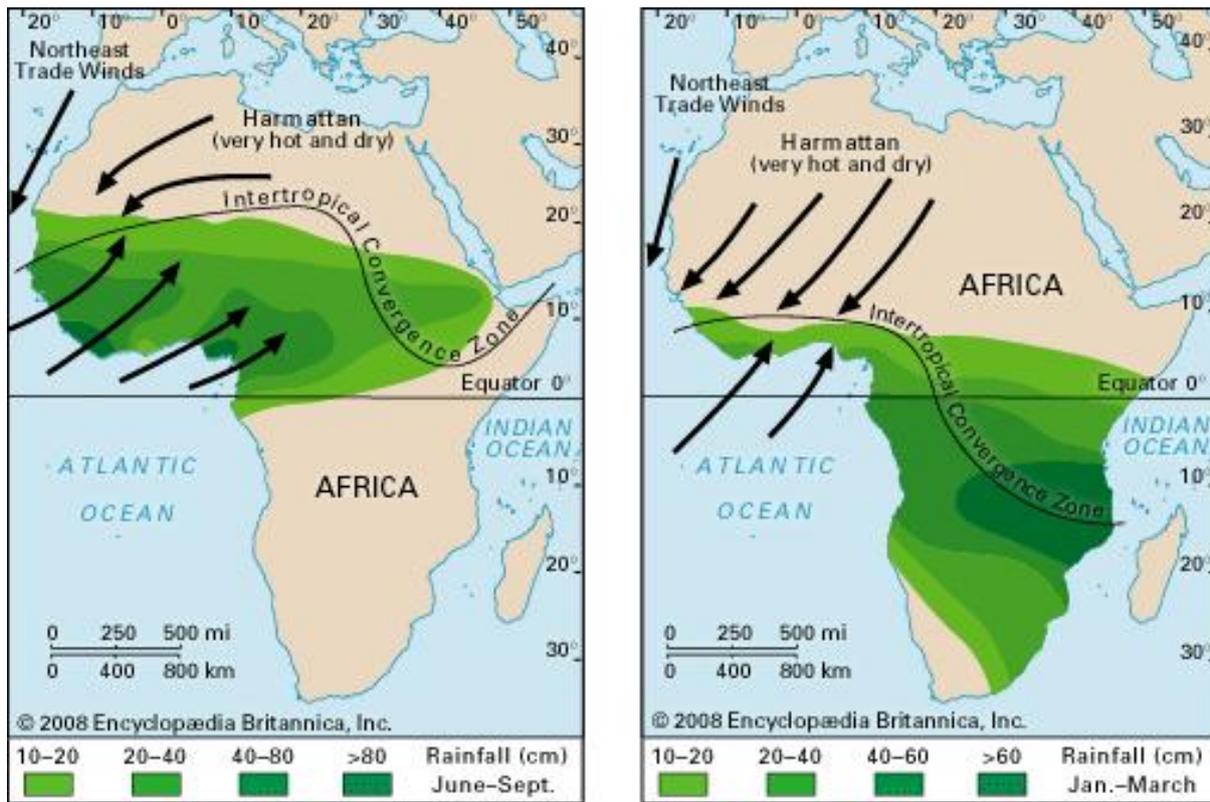
Figure 6: Seasonal distribution of precipitations due to the ITCZ shift and African Monsoon (Picture Credits: Climate and Ocean: Variability, Predictability and Change (CLIVAR))

The impact of detecting clouds more effectively is clearly visible in the period June-September north of the Equator (see Figure 7 and Figure 8) and in the period January-March south of the Equator (see Figure 9 and Figure 10). As expected, the introduction of an external cloud mask introduced a signature of clouds in the albedo fields resulting in a smaller number of albedo estimates that have better quality by removing unrealistically high albedo values leading to a reduction of temporal variability.
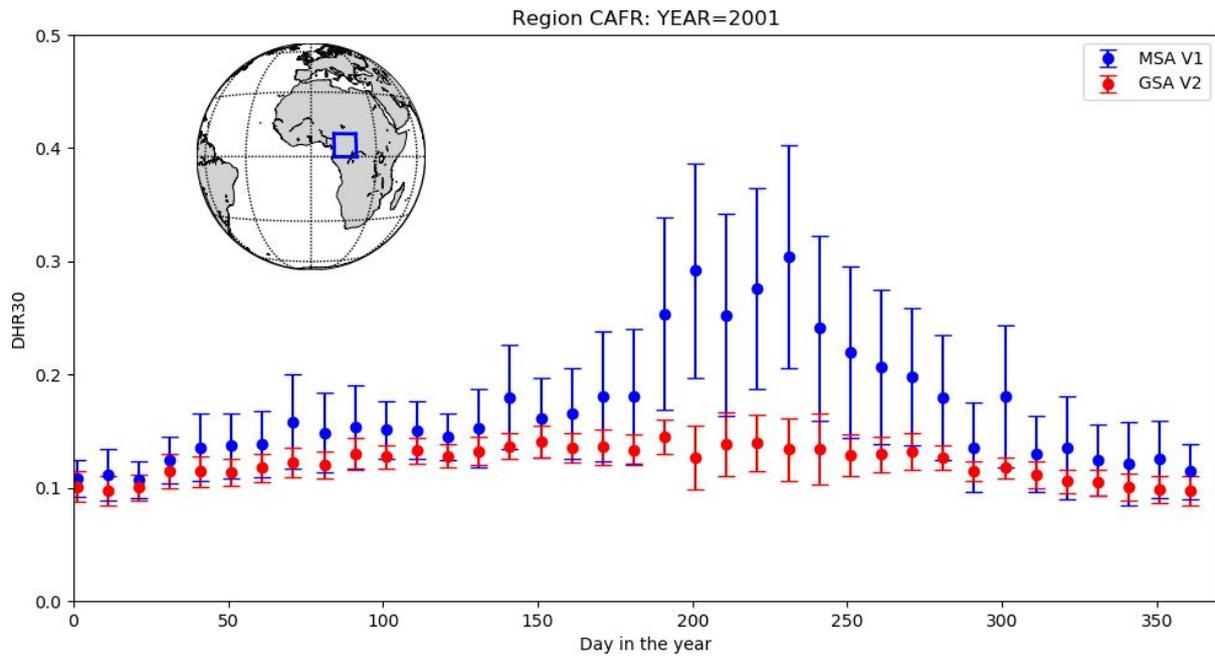
Figure 7: Comparison of DHR30 as retrieved in the displayed region for MSA Release 1 (blue) and GSA Release 2 (red).
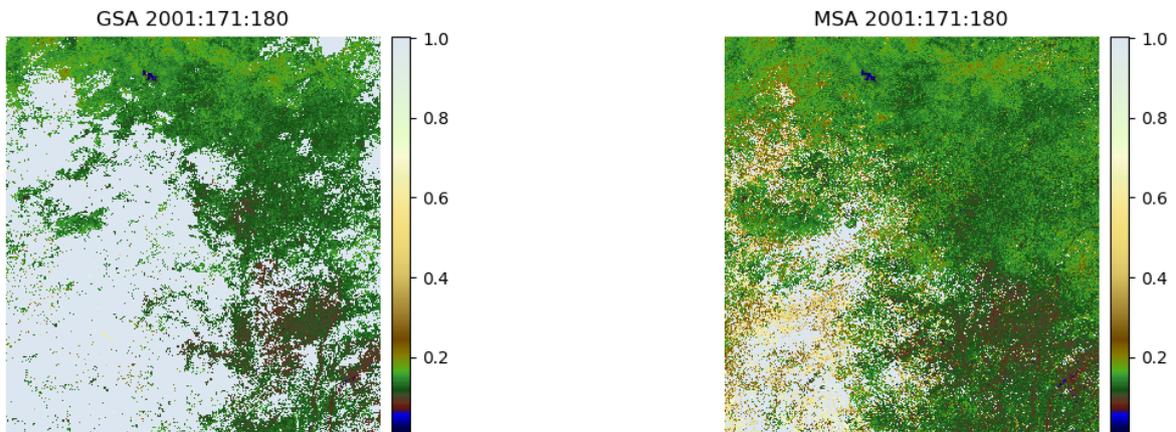

Figure 8: Map comparison between GSA Release 2 (left panel) and MSA Release 1 (right panel) for the period 171-180 (20th to 30th of June) 2001.
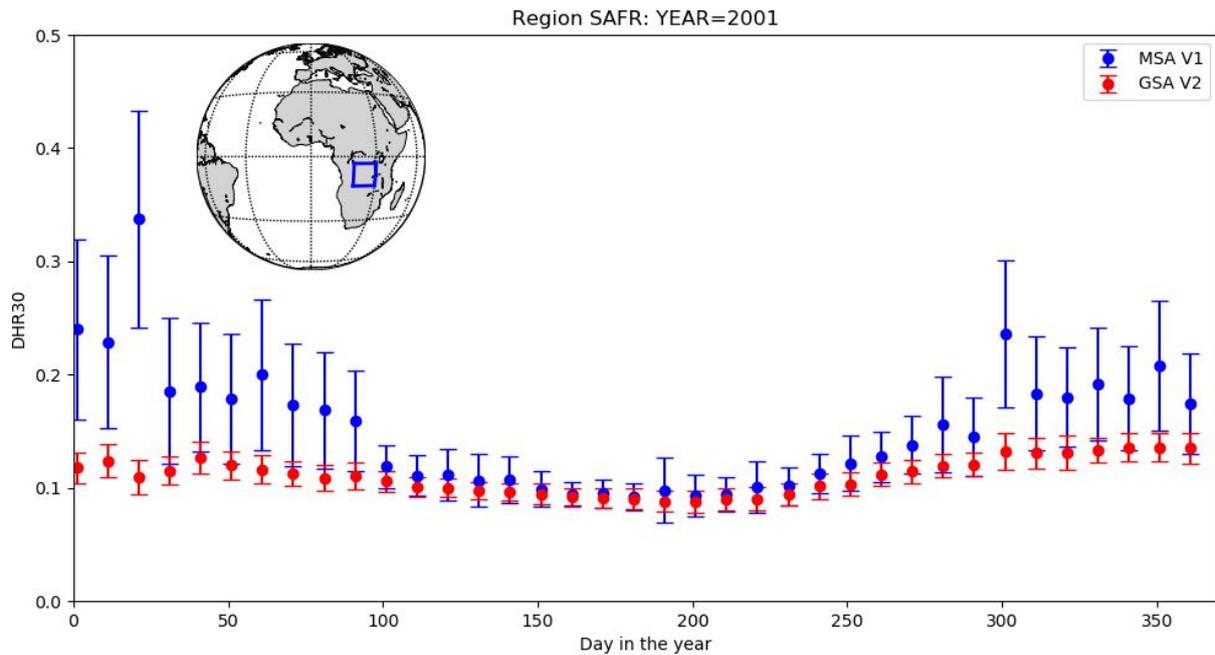
Figure 9: Comparison of DHR30 as retrieved in the displayed region for MSA Release 1 (blue) and GSA Release 2 (red).
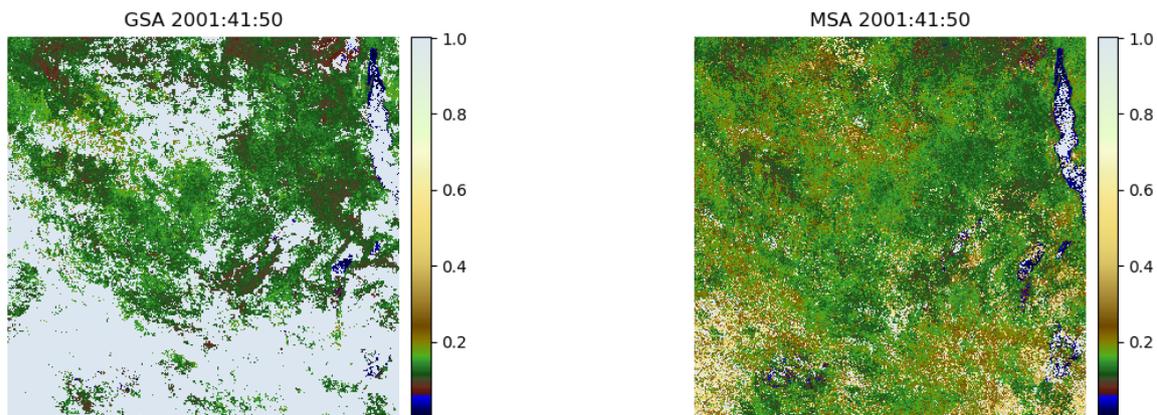

Figure 10: Map comparison between GSA Release 2 (left panel) and MSA Release 1 (right panel) for the period 041-050 (10th to 20th of February) 2001.

4.2   Time Series Analysis

In this section, the GSA data record is analysed in terms of self-consistency. Time series of the total/average values of key retrieval variables are estimated over the full disk for the complete periods for the three orbit positions (0°, 63°E, and 57°E) of MFG and for the 0° orbit position of MSG. The plots from top to bottom show:

- Absolute (red) and relative (blue) number of retrieved pixels
- DHR30 (black-sky albedo): spectral (red), retrieved uncertainty (shaded red), broadband (blue)
- BHRiso (white-sky albedo): spectral (red), broadband (blue)
- Average probability (red), average radiometric uncertainty (blue)
- Average Aerosol Optical Thickness (AOT)

These variables provide an overall picture of the goodness of the retrieval. The ATBD [AD2] explains in detail the meaning of the different variables.
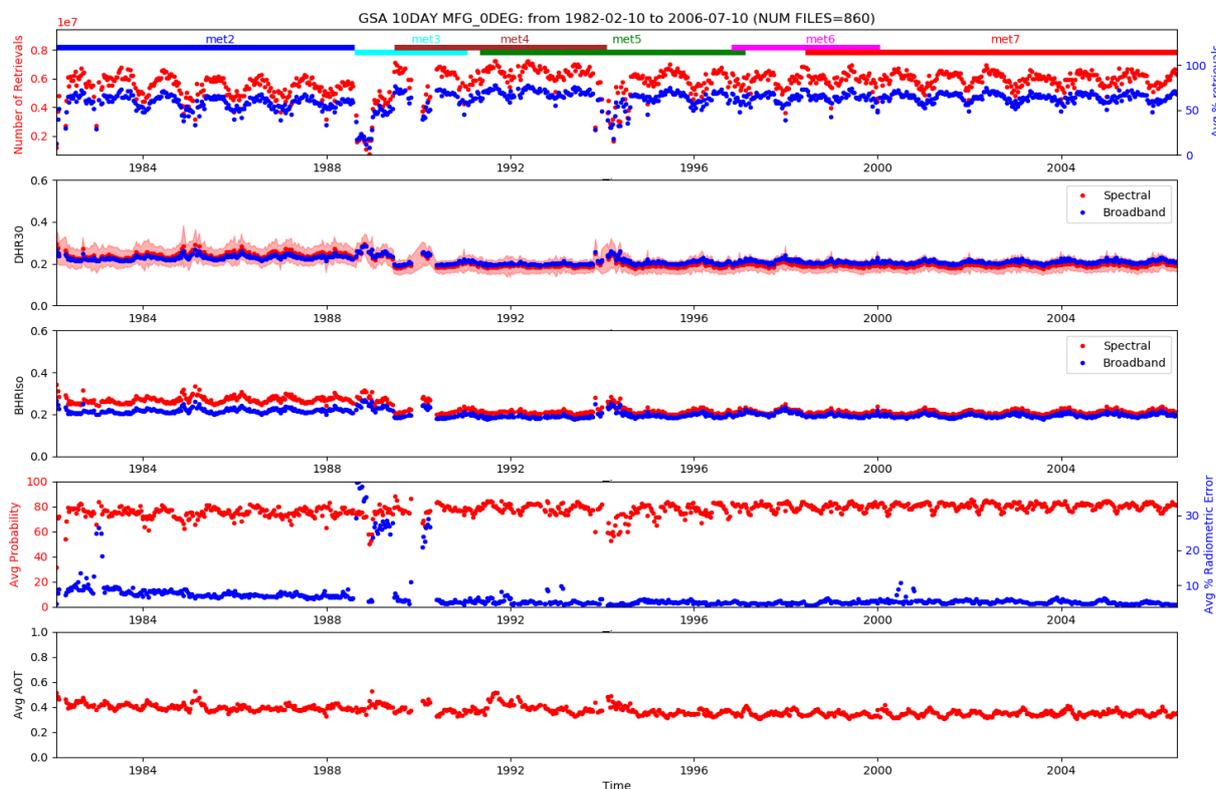

Figure 11: Time series of full disk averages of variables derived from Meteosat First Generation measurements at 0° orbit position throughout the entire mission.

The temporal analysis at full disk level shows a very good stability of the retrieval for all orbit positions (MFG 0°, 63°E, 57°E and MSG 0°). The average number of product retrieval is always between 50% and 85%. The average radiometric error (uncertainty in the input imagery) is between 3 and 8% and the average probability of the retrievals for all cases is close to 80%. These values provide an estimation of the input quality (affecting the retrieval uncertainty) and a general confidence level in the solution quality. The average AOT is very similar for MFG (Figure 11) and MSG (Figure 14) at 0° and it is in the range [0.38-0.4]. For MFG at 57° (Figure 13) and 63° (Figure 12) the value is ~0.3.

From Figure 11 an anomalous behaviour for Meteosat-3 in the first quarter of 1990 can be identified. The number of retrievals drops down with a significant higher DHR30 and a very high average radiometric uncertainty. This is due to an issue with the input imagery. Several images (level 1.5 data) are not available and the VIS 1 detector was available only for odd slots for the whole Meteosat-3 lifetime to fix an issue with the water vapour channel on the same platform. Also for Meteosat-2 the VIS 1 detector was available only for odd slots its whole lifetime[4]. The decreased amount of input measurements has of course an impact on the quantity and quality of

---

[4] MFG gain information (link valid 03/04/2020):
https://www.eumetsat.int/website/home/Data/ServiceStatus/MeteosatGainSettings/index.html

the retrieved surface albedo. A decrease in the retrieval probability (<80%) or an increase in the radiometric error (>15%) or an increase in the overall uncertainty (>15%) would provide an indication of limited quality that each user should assess.
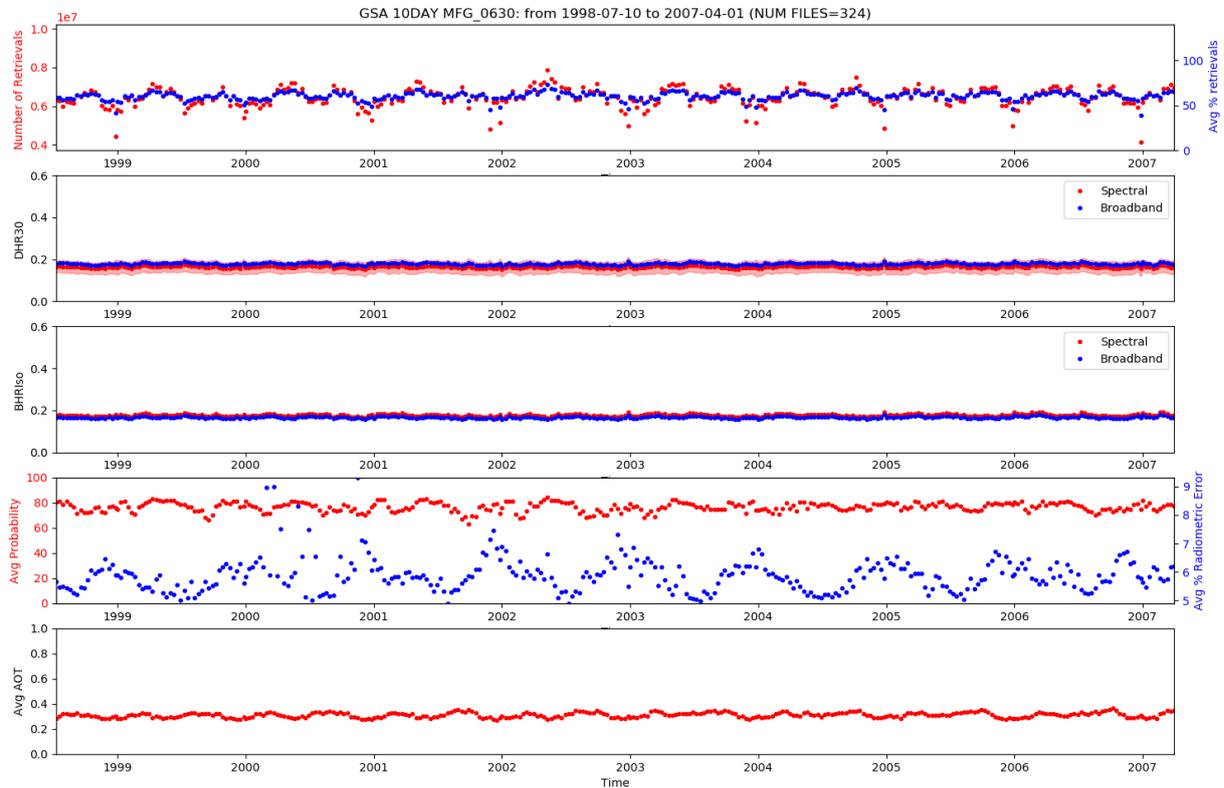

*Figure 12: Same as Figure 11 but for 63°E orbit position (only Meteosat-5).*
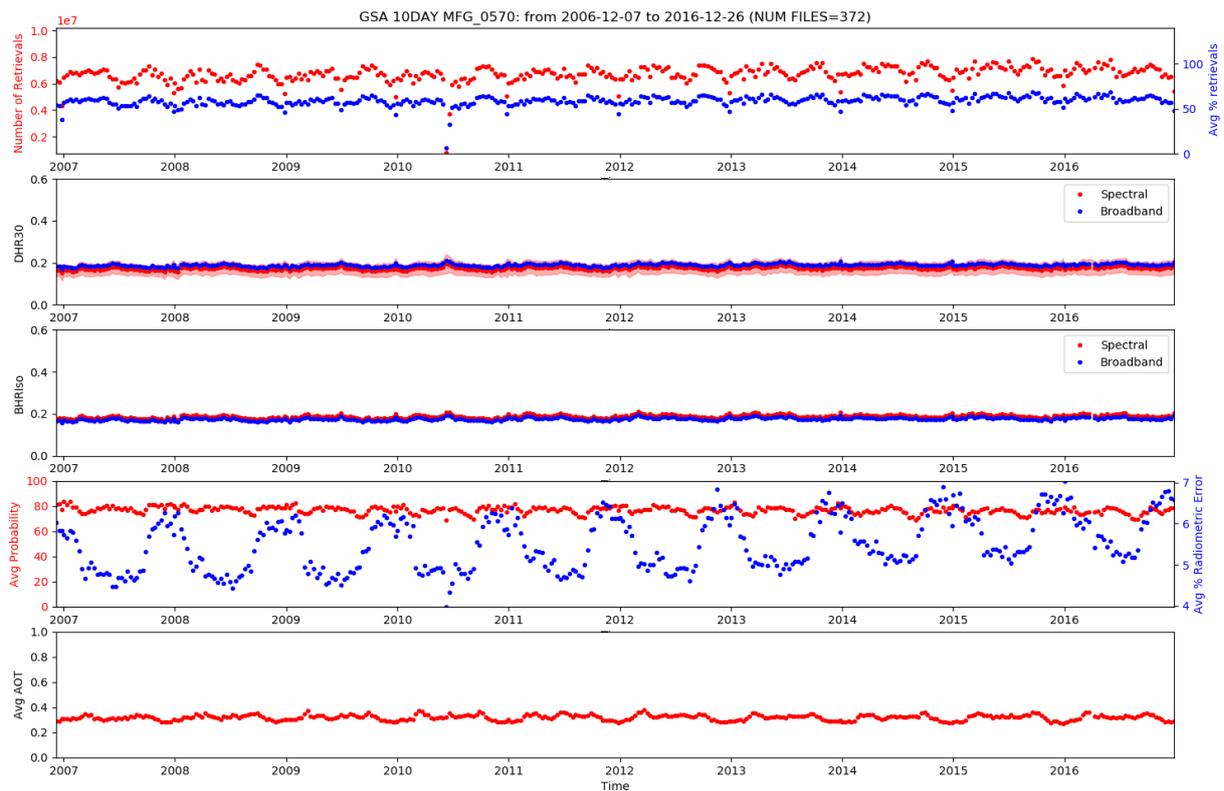
*Figure 13: Same as Figure 11 but for 57°E orbit position (only Meteosat-7).*
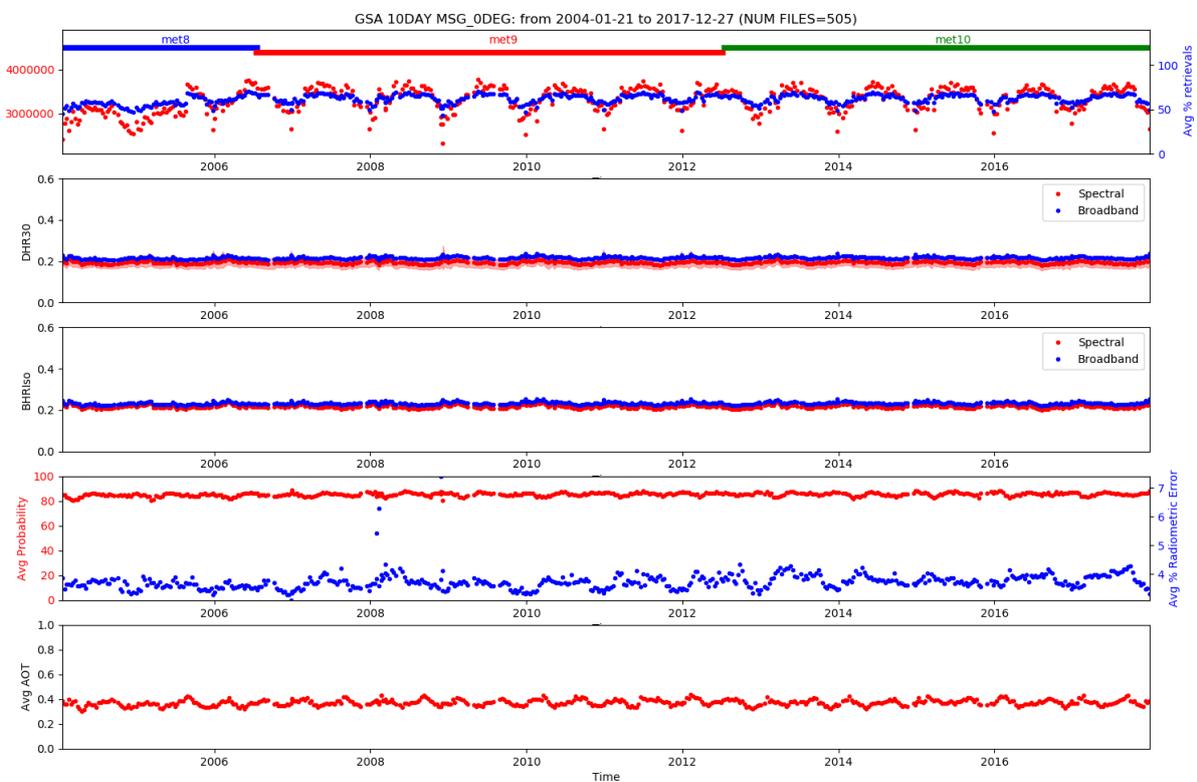
Figure 14: Same as Figure 11 but for Meteosat Second Generation 0° orbit position.

In order to assess the data record's temporal stability at pixel level, several time series for some SAVS targets (Table 4) have been generated. The albedo over three of those targets (SOV, LIBIA_00001, MORZUQ_DESERT) is expected to remain stable over time. MONGU (urban site) and SKUKUZA (Shrubland) have been selected to show temporal variations over different surface types. Meteosat acquires the portion of the Earth where these targets are located at different viewing angles. SOV is close to the disk edge (higher satellite viewing angle), while the others are closer to the sub satellite point (lower satellite viewing angle). Figure 15 to Figure 18 show the temporal variation of the DHR30 (spectral in red and broadband in blue) from Meteosat-2 to Meteosat-10. The regression line is in green. The spectral values for Meteosat-2 and Meteosat-3 are clearly higher. This effect is due to a problem with the calibration of the VIS channel. The effect is in percentage, so it is more pronounced for high DHR30 values. The conversion to broadband attempts to mitigate this problem [RD2].
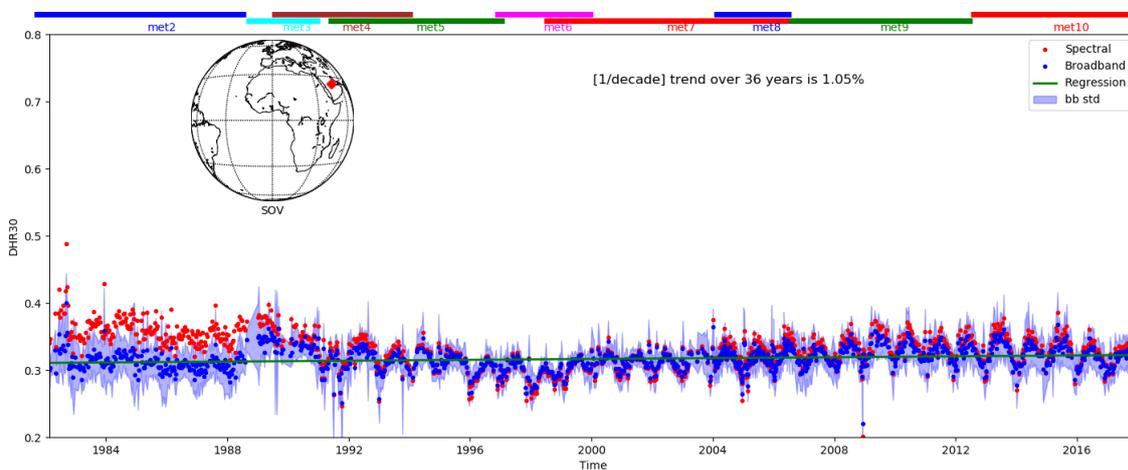

Figure 15: Time series of DHR30 (black-sky albedo) at site SOV (location shown in red on the map). The spectral albedo value is in red, the broadband albedo in blue (its standard deviation shaded blue) and the regression line for the trend in green. On the top of the plot, the available Meteosat satellites are indicated but only one (the operational) is used to construct the time series.
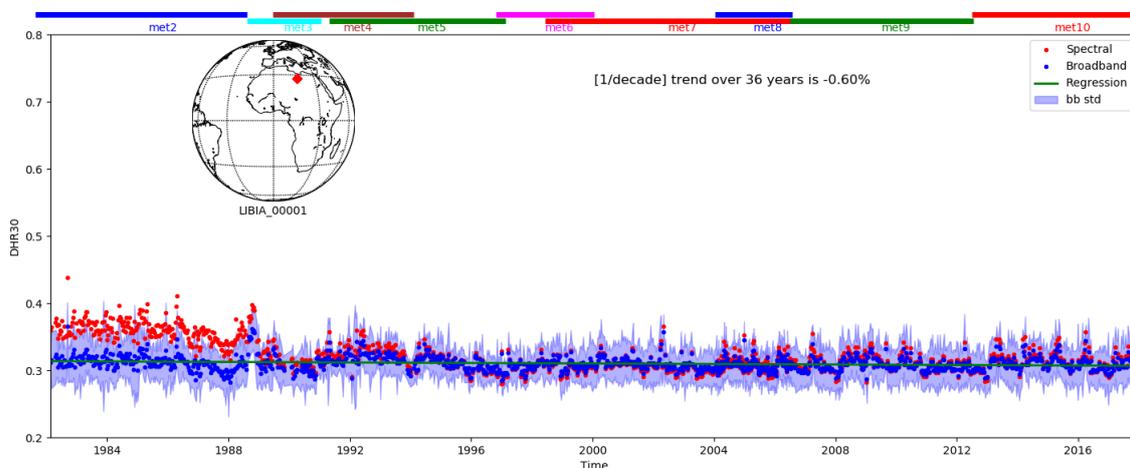

*Figure 16: Same as Figure 15 but at site LIBIA_00001.*
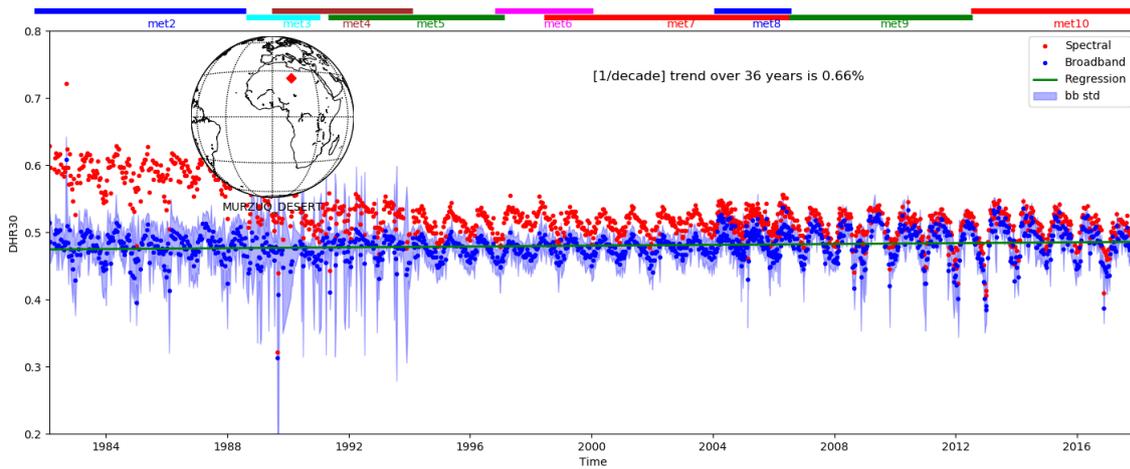
Figure 17: Same as Figure 15 but at site MORZUQ_DESERT. The high spectral values for Met-2 are due to an issue with the VIS channel calibration. The broadband conversion is able to correct it almost entirely.
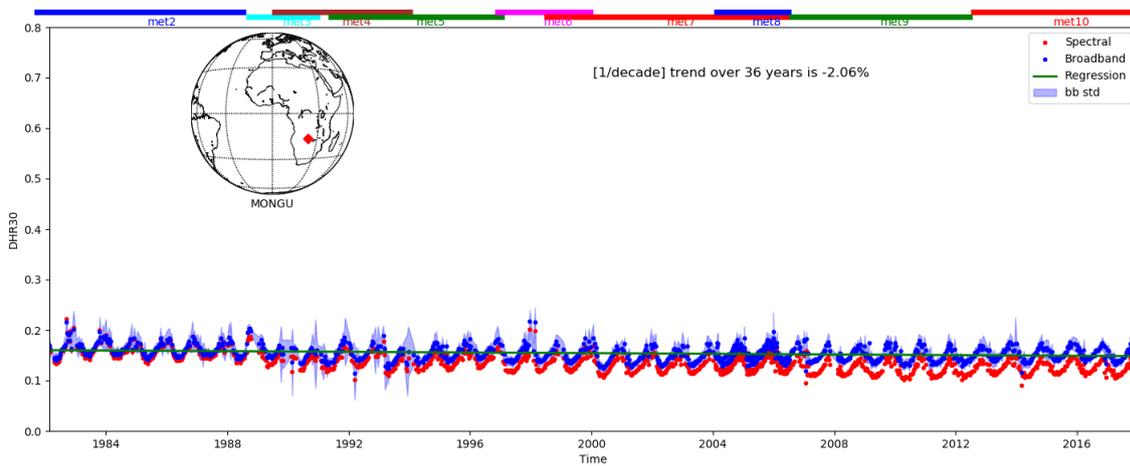

*Figure 18: Same as Figure 15 but at site MONGU.*
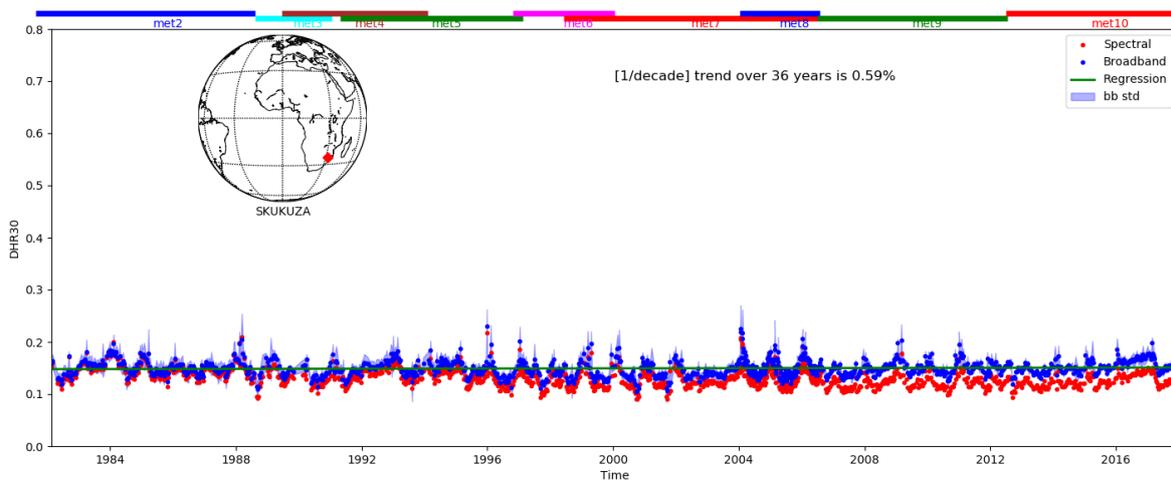
Figure 19: Same as Figure 15 but at site SKUKUZA.

The decadal trend over more than thirty-six years and nine different satellite instruments is close to 1% with the only exception of the MONGU site (see Table 5). This site is classified as "urban" and there is no specific reason to expect a stable albedo over thirty-six years

SITE NAME	DECADAL TREND
SOV	1.05%
LIBIA_00001	-0.6%
MORZUQ_DESERT	0.66%
MONGU	-2.06%
SKUKUZA	0.6%

Table 5: Broadband DHR30 decadal trend over thirty-six years over desert and urban validation sites.

4.3   Spatial Overlap Analysis

In order to assess the retrieval consistency among the missions operating at the same and different orbital positions, a comparison for a longitudinal transect averaged over a specific month (April 2005) has been performed for the broadband DHR30 (or black-sky albedo). In order to minimize the potential discrepancies due to a different viewing geometry, a transect at the longitude of 31.5°E has been chosen. This value marks exactly the middle between the nominal locations of the 0° orbit position (for both MFG and MSG) and the IODC orbit position at 63°E.
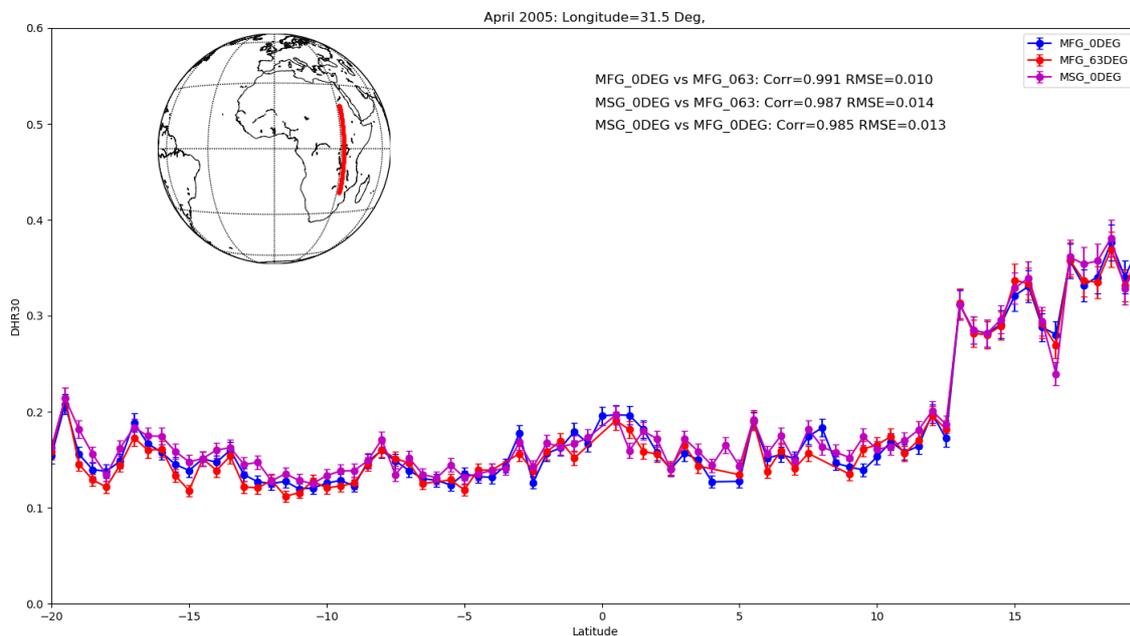
Figure 20: Comparison between the broadband DHR30 retrieved along a longitudinal transect from Meteosat-7 (blue), Meteosat-5 (red) and Meteosat-8 (magenta).

Figure 20 demonstrates good agreement between all four Meteosat estimates including the comparison of the first (Meteosat-5 and -7) and second-generation (Meteosat 8) satellites estimates. The DHR30 correlation is always higher than 0.98. Table 6 contains the correlation, the Mean Absolute Error (MAE) and Root Mean Square Error (RMSE) for each comparison. PERC is the percentage relative RMSE with respect to the DHR30 average over the transect that

is 0.19 for all cases. Analysis for other periods (not included in this report) exhibit very similar results.

Pair	Correlation	MAE	RMSE	PERC
MFG_0DEG vs MSG_0DEG	0.985	0.010	0.013	7.0
MFG_0DEG vs MFG_IODC	0.991	0.0079	0.0099	5.4
MSG_0DEG vs MFG_IODC	0.987	0.012	0.014	7.6

Table 6: Statistics of the DHR30 comparison among MFG 0DEG, MFG 63DEG and MSG 0DEG over the longitudinal transect at 31.5°E. The average DHR30 is 0.19.

Both MAE and RMSE are expressed in albedo units and can be directly compared. A smaller the difference between MAE and RMSE means that the uncertainty in the DHR30 time series can be represented by a random distribution. This is true for all cases. Case 2 shows a MAE and RMSE lower than the corresponding values for Case 1 and Case 3. This might be expected because Case 2 compares retrievals performed with the same instrument (MVIRI) even if on different platforms (MET-7 at 0°and MET-5 at 63°E).

5   VALIDATION AGAINST A REFERENCE

This section describes the black sky albedo (DHR30) comparison over the five selected SAVS sites. The discussion is split into a qualitative comparison based on the time series and a quantitative one based on the RMSE and MAE values. A filter based on the median absolute deviation [RD20], with a cut-off of three, is exploited to detect outliers in the time series. Outliers for GSA are most likely due to undetected clouds. The fact that outliers are values higher than the range of annual variation supports this hypothesis. The persistence of some minor remaining cloud contamination in the GSA data record after the exploitation of an external cloud mask is further discussed in the report conclusions.

The values shown from Figure 20 to Figure 30 represent the average over a 5x5 pixels around the site location and the error bar is the standard deviation for that area. All Figures share the same y-axis interval in order to make them directly comparable. The location of the target on the Meteosat disk is shown in each figure as well. The agreement shown in the plots is very good for bright desert (Figure 22 to Figure 28) targets (<7%) and good for urban (Figure 29) and forest targets (Figure **31**) (between 8% and 9%).

MODIS and GSA DHR30 only consider the direct component (DHR) of the albedo and therefore exhibit slightly lower values compared to the SAFARI campaign observations, containing also the diffuse fraction.
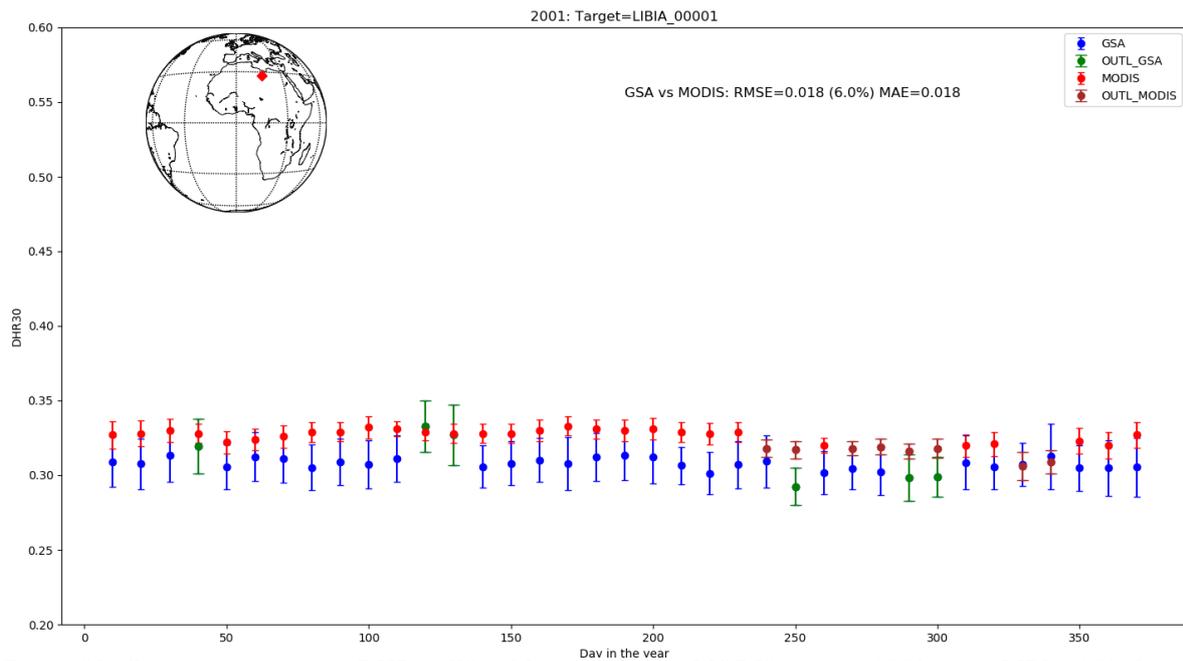
Figure 21: Comparison between DHR30 GSA (Meteosat-7) and MODIS for year 2001 at the LIBIA_00001 site. GSA is denoted in blue, GSA outliers in green, MODIS in red, MODIS outliers in brown.
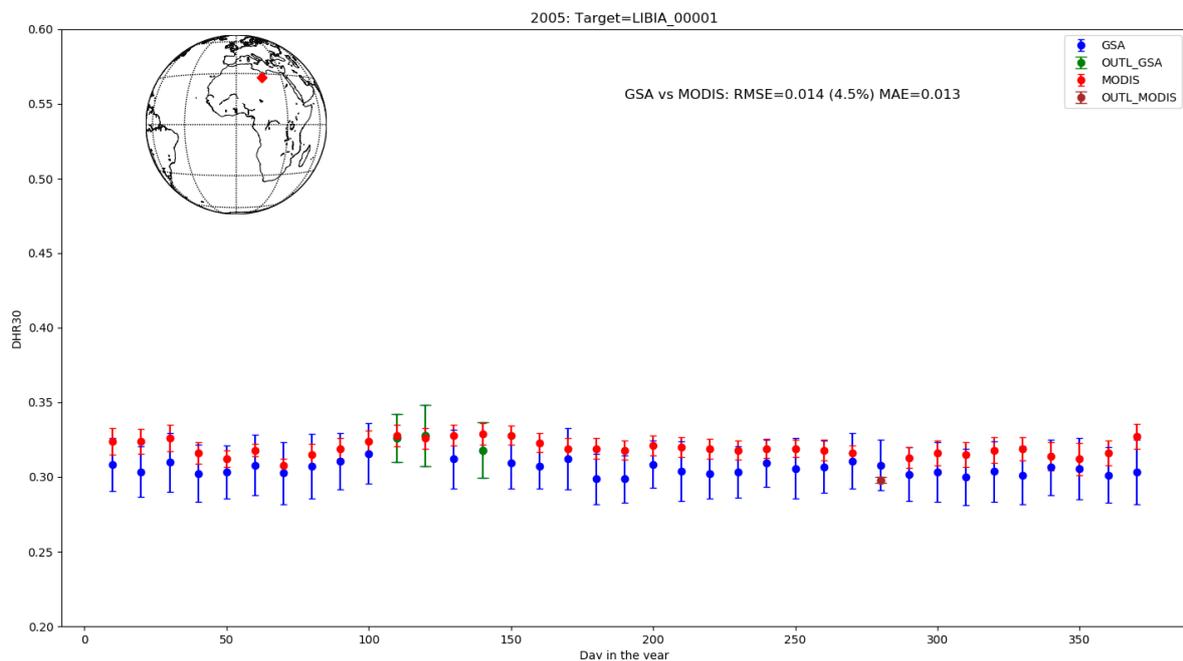

Figure 22: Same as Figure 21 *but using Meteosat-8 and for year 2005 at the LIBIA_00001 site.*
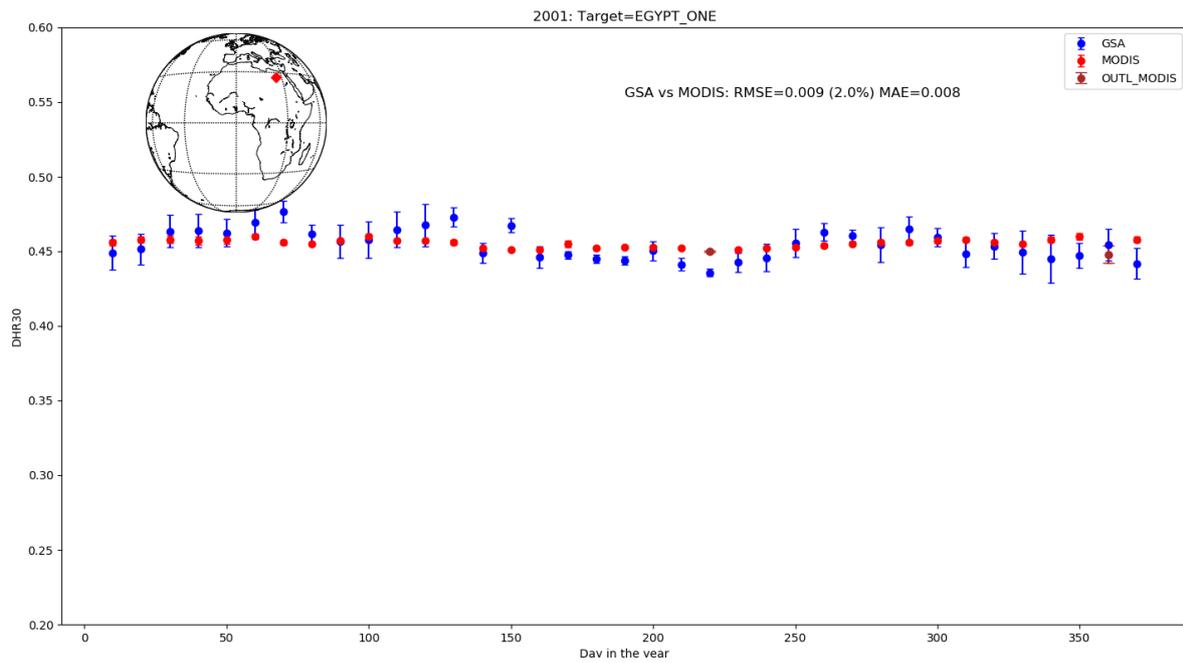
Figure 23: Same as Figure 21 using Meteosat-7 and for the year 2001 at the EGYPT_ONE site.
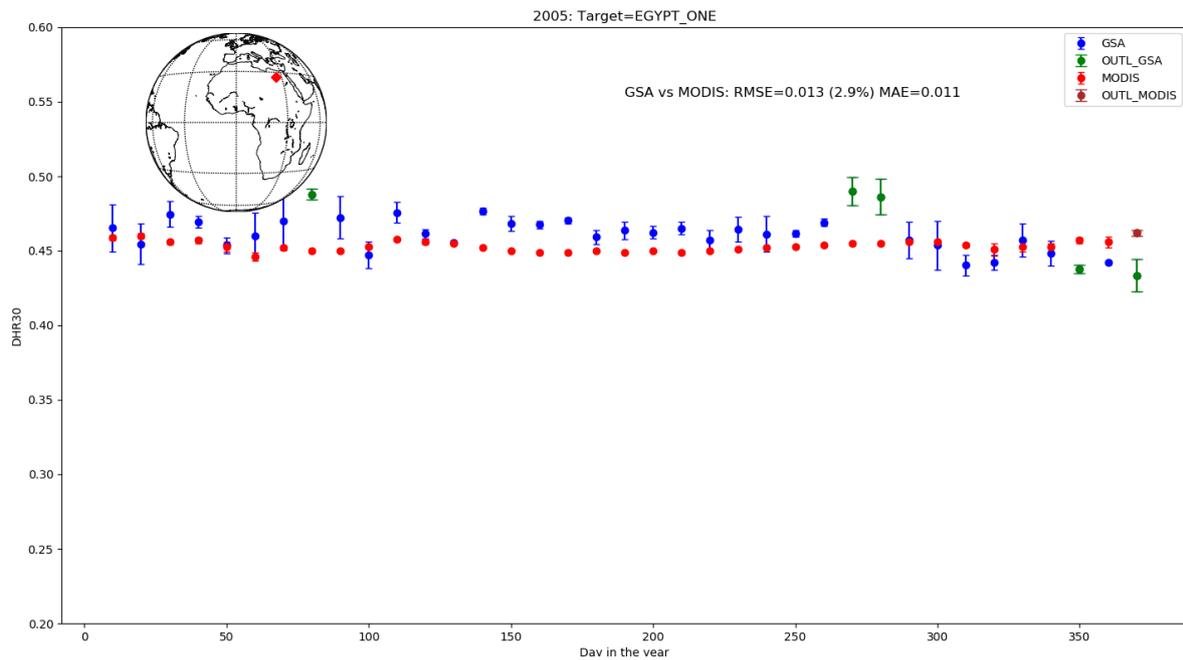
Figure 24: Same as Figure 22 using Meteosat-8 and for year 2005 at the EGYPT_ONE site.
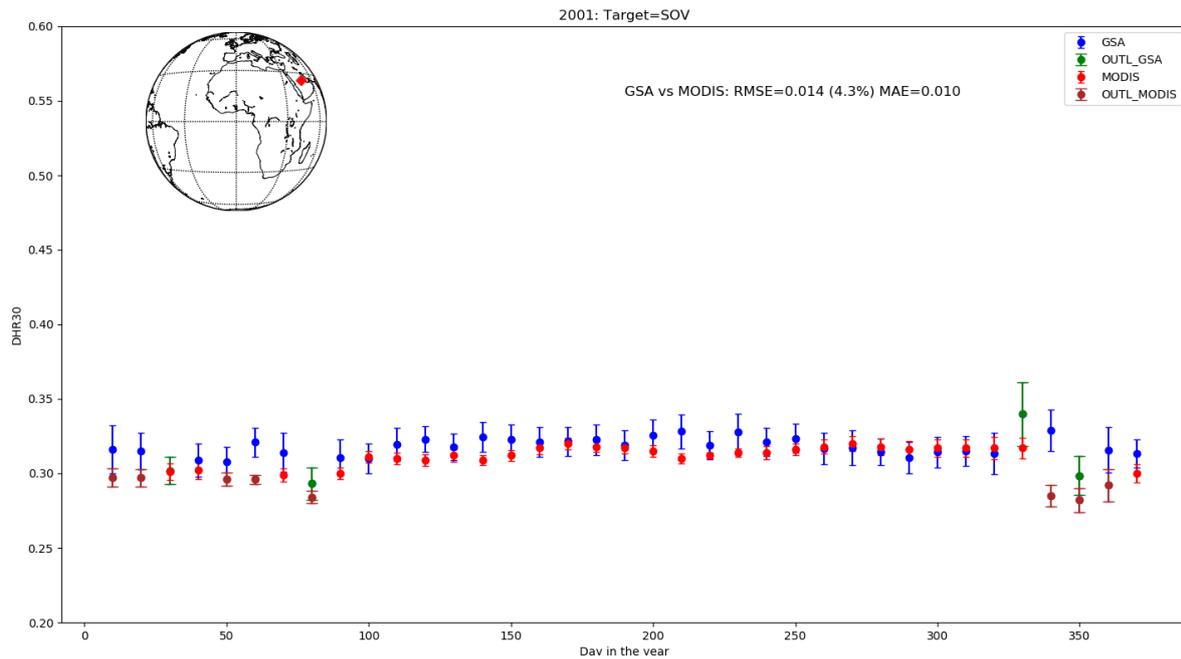
Figure 25: Same as Figure 21 for Meteosat-7 for the year 2001 at the SOV site.
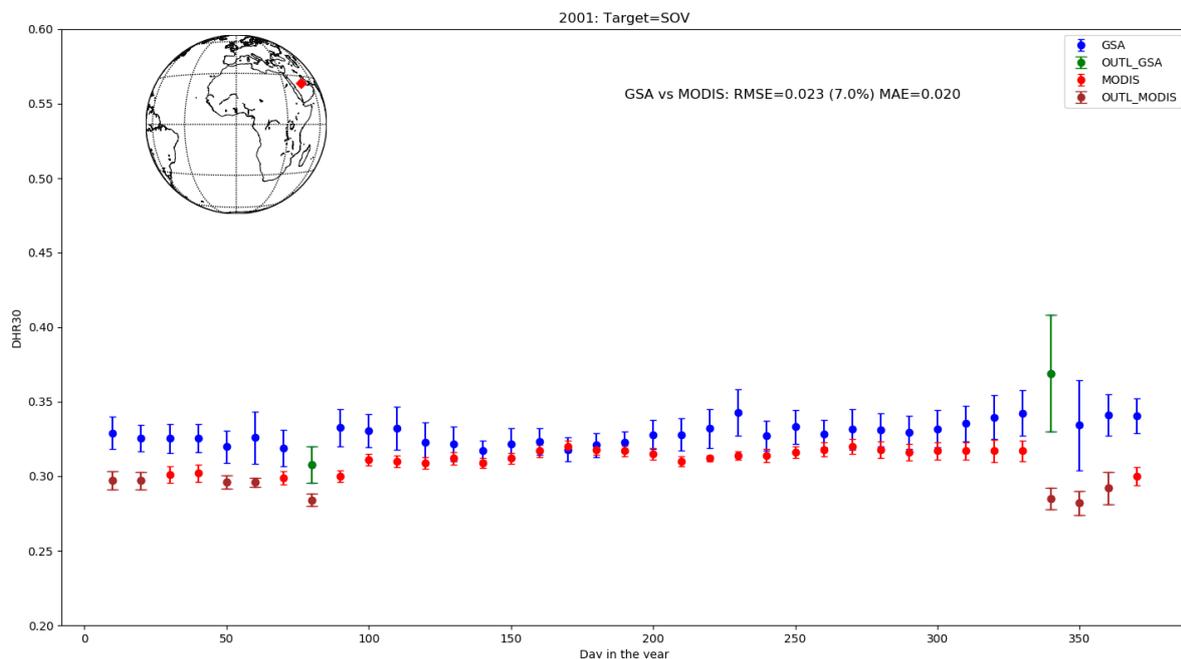
Figure 26: Same as Figure 21 for Meteosat-5 for the year 2001 at the SOV site.
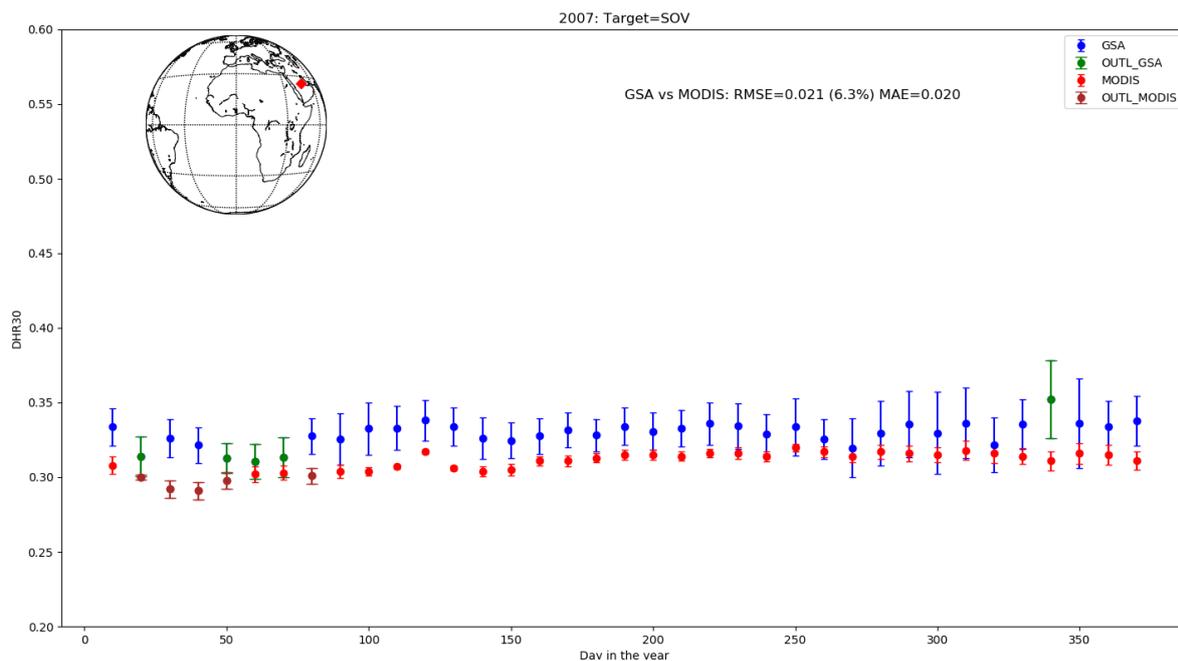
Figure 27: Same as Figure 21 for Meteosat-7 for the year 2007 at the SOV site.
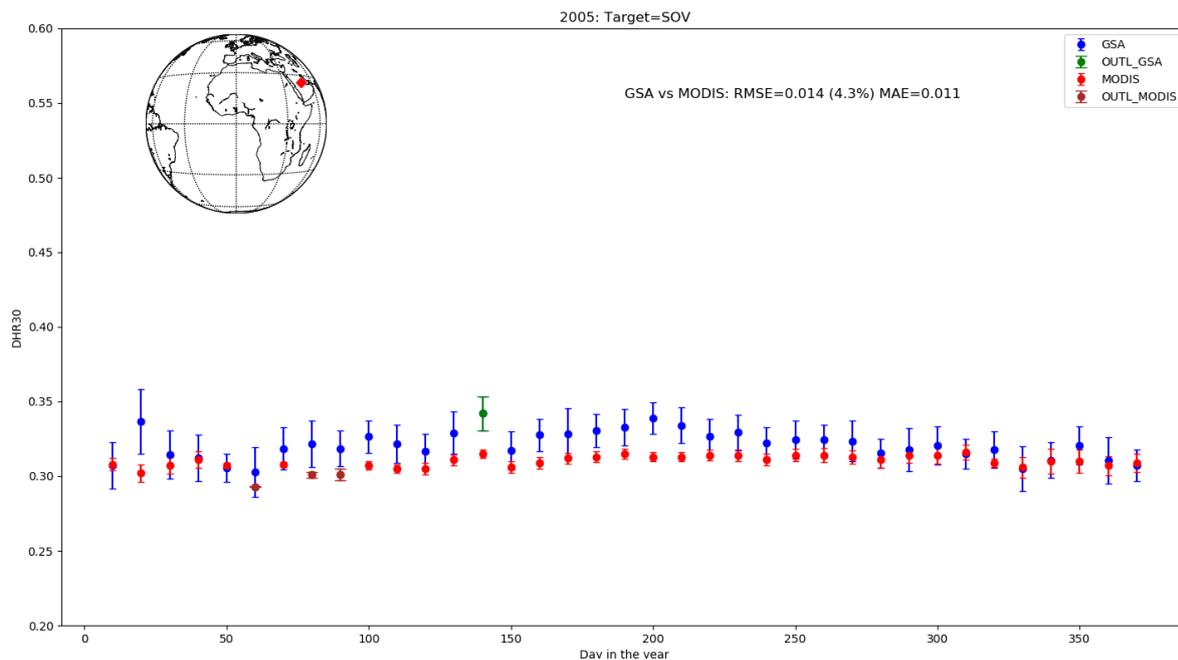
Figure 28: Same as Figure 21 for Meteosat-8 for the year 2005 at the SOV site.
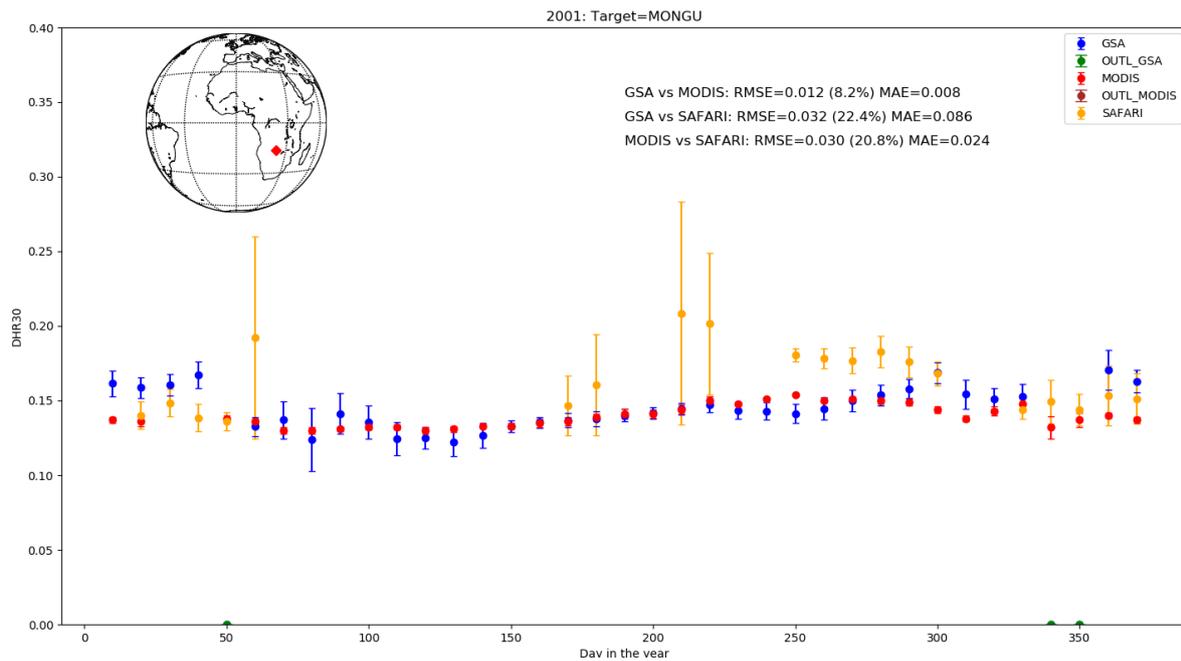
*Figure 29: Comparison between GSA (Meteosat-7), MODIS and SAFARI for the year 2001 at the MONGU site. SAFARI data in yellow. GSA and MODIS are plotted as black-sky albedo (DHR30), while SAFARI is represented as blue-sky albedo (BHR).*
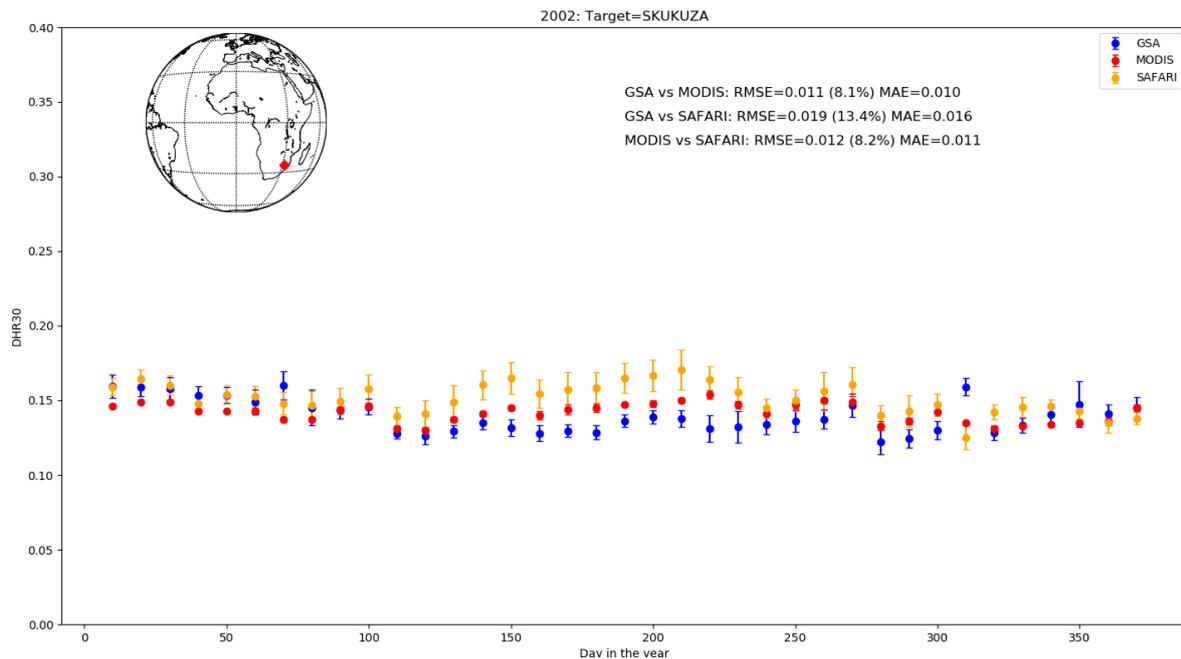
Figure 30: Comparison between GSA (Meteosat-7), MODIS and SAFARI for the year 2002 at the SKUKUZA site. SAFARI data in yellow. GSA and MODIS are plotted as black-sky albedo (DHR30), while SAFARI is represented as blue-sky albedo (BHR).
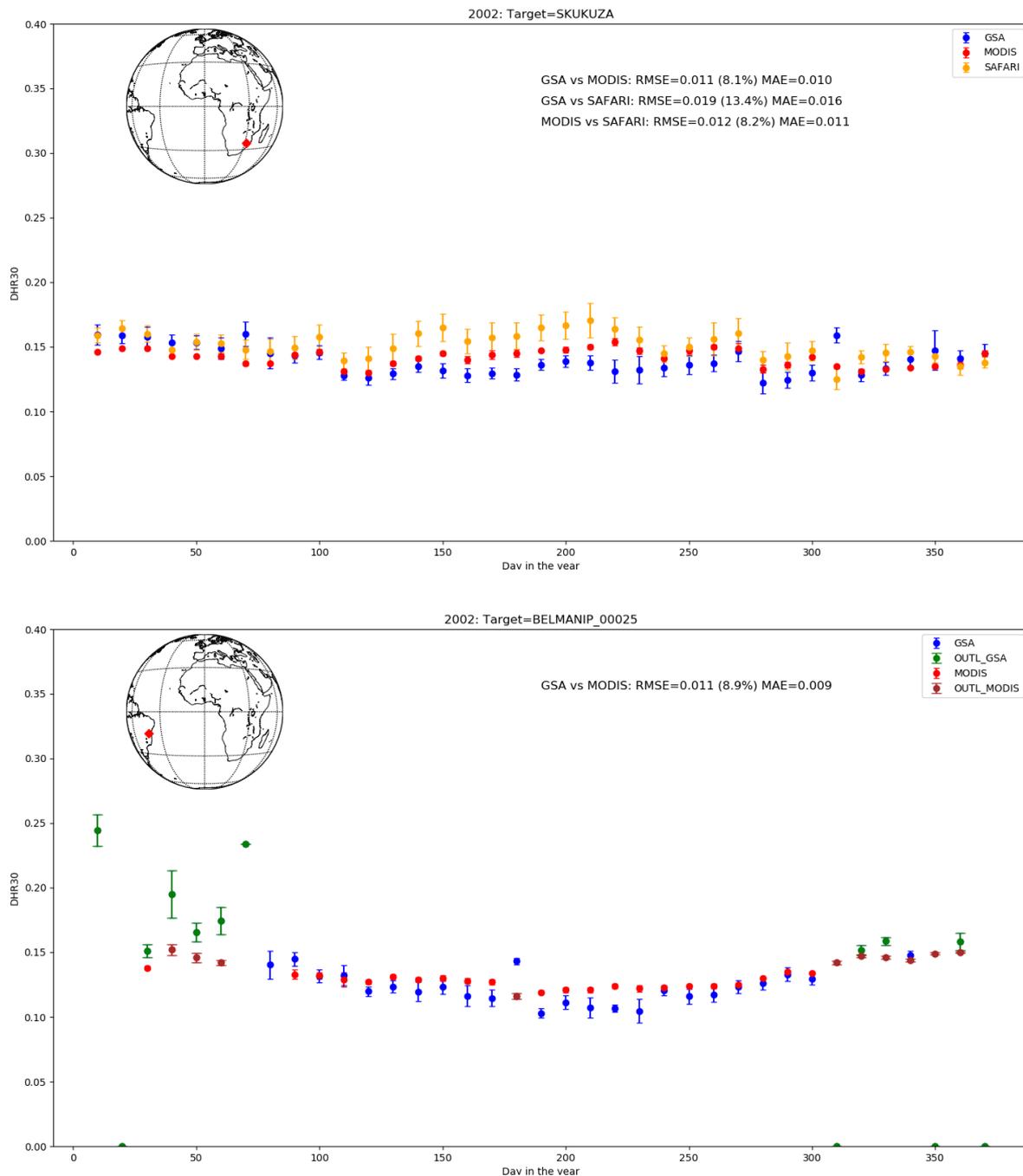
Figure 31: Comparison of GSA (Meteosat-7) vs. MODIS for the year 2002 at the BELMANIP_00025 site.

Table 7 presents the quantitative comparison for all targets using RMSE and MAE as the major measures of quality. The RMSE and MAE were calculated excluding the outliers. PERC is the percentage relative RMSE with respect to the DHR30 average (AVG) calculated over the sample (SAMP) values (the maximum is 37, i.e. the maximum number of GSA products for a year). In addition, Table 8 shows the quantitative comparison to SAFARI data at the MONGU and SKUKUZA sites.

NAME	YEAR	SATID	AVG	SAMP	RMSE	PERC	MAE
LIBIA_00001	2001	Meteosat-7	0.308	31	0.018	6.0	0.017
	2005	Meteosat-8	0.305	34	0.014	4.5	0.013
EGYPT_ONE	2001	Meteosat-7	0.455	37	0.009	2.0	0.008
	2005	Meteosat-8	0.461	32	0.013	2.9	0.011
SOV	2001	Meteosat-7	0.318	33	0.014	4.3	0.010
	2001	Meteosat-5 (IODC63)	0.329	35	0.023	7.0	0.020
	2005	Meteosat-8	0.320	36	0.014	4.3	0.011
	2007	Meteosat-7 (IODC57)	0.331	32	0.021	6.3	0.020
MONGU	2001	Meteosat-7	0.143	32	0.012	8.2	0.0084
SKUKUZA	2002	Meteosat-7	0.140	37	0.011	8.1	0.0096
BELMANIP_00025	2002	Meteosat-7	0.122	23	0.01	8.9	0.0089

Table 7: RMSE, PERC and MAE between DHR30 GSA and MODIS for the selected targets and periods. Values were computed using 5x5 Meteosat pixels around the site location. AVG is the GSA average value. Statistics calculated over SAMP values.

SITE	Comparison	YEAR	SATID	AVG	SAMP	RMSE	PERC	MAE
MONGU	GSA vs SAFARI	2001	Meteosat-7	0.152	17	0.032	22.4	0.086
	MODIS vs SAFARI	2001	MODIS	0.1	18	0.029	20.8	0.024
SKUKUZA	GSA vs SAFARI	2002	Meteosat-7	0.140	37	0.019	13.4	0.086
	MODIS vs SAFARI	2002	MODIS	0.141	37	0.012	8.2	0.011

Table 8: As Table 7 but for SAFARI BHR data.

The comparison against MODIS and SAFARI data (from Figure 20 to Figure 31 and Table 7) shows a RMSE between 2% and 7% for bright desert sites and around 8% for MONGU and SKUKUZA. The worst agreement is for BELMANIP_00025 where the RMSE is 8.9%

6 LIMITATIONS

The GSA retrieval scheme can be applied to a wide set of geostationary satellites ([RD13] and [RD19]). It has been developed to exploit imagery acquired by old imagers having an extremely limited spectral radiometric capacity. The usage of such old instruments necessarily introduces some intrinsic limitations. GSA attempts to mitigate the impact of such limitations providing the user with some control parameters such as the uncertainties and the probability of the solution set. The radiometer on board the MFG satellites acquires radiances twice (MSG four times) per hour in a single large solar spectral band ranging from 0.4 µm up to 1.1 µm (see Figure 2). This interval contains some gas absorption bands and is subject to aerosol scattering-absorption processes whose magnitude depends on the wavelength. Because of that, the decoupling between absorption and scattering processes done in the retrieval introduces some inaccuracies due to the integration

over such a large spectral interval. Vegetation reflectance exhibits strong and fast variations over the spectral region 0.4 µm - 1.1 µm because of the differences in the radiation transfer regimes occurring on both sides of 0.7 µm. This is mainly driven by absorption at wavelengths shorter than 0.7 µm and by scattering at larger wavelength.

These spectral variations cannot be explicitly considered in the atmospheric-correction scheme because observations occur only in one single band. Consequently, surface albedo derived from geostationary satellite observations in the VIS band with the GSA algorithm is subject to some systematic biases depending on the shape of the surface spectra, the aerosol load, and the absorbing gas concentration.

A limitation for Meteosat Second Generation is due to the change of scanning mode during the time of operations[5]. From 31 August 2005 onwards, the lower window of the HRV channel was shifted to follow the daily illumination, while it was fixed over Africa before this date. For this reason, for periods before 31 August 2005, no retrieval of South America is possible with MSG HRV imagery. At high view zenith angle (far from the sub satellite point), the geostationary projection introduces a distortion in the pixels and the path thought the atmosphere is longer. This combination of factors implies a lower reliability in both the cloud detection and albedo retrieval. The uncertainty and associated probability estimated at pixel levels try to account for that. The user should pay particular attention to those areas. This effect is more relevant in case of areas subject to an on average high cloud coverage like Amazonia.

The introduction of an external cloud mask improved significantly the quality of the data record compared to the previous version. Some cloud contamination is still present. A possible solution to overcome this and to further remove the remaining cloud contamination in the retrieved albedo data record could be the approach presented in [RD17]. Here it is proposed to create a climatological seasonal background (cloud free) albedo from the GSA data record itself. The usage of an external climatological value, depending on a different aerosol retrieval, could introduce albedo variations due to a different estimation of the coupled albedo-aerosol system that might be taken as real changes. The retrieved DHR30 is compared against the climatological background and values 40% higher than the background should be removed. Being based on a threshold comparison with a climatological background, this post-processing could remove good retrievals. For a climate data record, it is preferable to have a limited number of retrievals but with the highest possible quality and reliability rather than a greater volume of less reliable data. This approach could have a negative impact on snow-covered single pixels, so removing sporadic snow falls should then be carefully considered taking into account the user's objective.

The range of variation allowed for the Aerosol Optical Thickness (AOD) in the look-up tables [AD3] might lead to a higher albedo due to the saturation of the aerosol contribution (AOD > 1) in the coupled system. The analysis of the AOD has been addressed for Release 1 [AD1] and it is valid for Release 2.

No atmospheric correction is performed depending on the pixel elevation. This can lead to an underestimation of the coupled surface-aerosol system because the air column is thinner than assumed. Though, this effect will only affect areas like the Himalaya region or the highland in South Africa.

---

[5] Details can be found here: https://www.eumetsat.int/website/home/Data/0DegreeService/index.html (Link valid 09/03/2020)

7   CONCLUSIONS

Black sky and white sky albedo, together with uncertainties, have been generated for both the first (MFG) and the second (MSG) generation of the EUMETSAT Meteosat satellites over a period of 36 years, from 1982 to 2017 for the main mission at 0 degrees. Data records for the IODC mission at 57°E and 63°E, covering a period of 19 years, have been also generated and validated. The retrieval processor applied is the same for both types of platform (MFG and MSG) and for all three missions (see [RD9], [RD10], [RD12]).

The data records for the various satellites at different orbit positions exhibit a very good stability over the full period both looking at the overall disk average (from Figure 11 to Figure 14). This analysis is providing a general monitoring of the data record over the complete temporal coverage. The analysis at specific validation sites (from Figure 15 to Figure 18) is quantitative, providing a value about the temporal stability. The decadal trend is less than 1% for the desert targets as expected. Also the decadal trend for the shrubland site is well below 1%.The urban site MONGU in southern Africa presents a trend >2% and a clear seasonal variation. However, this site by definition (urban site) is not supposed to show a stable behaviour over such a long time-range.

The analysis of the spatial overlap (Figure 20 and Table 6) shows a high consistency among the data records derived from the different satellites and from different orbit positions (MFG 0°, MSG 0°and MFG IODC 63°E). The correlation is close to 0.99 and the RMSE is around 7%.

The validation against external reference shows a good agreement with MODIS. The difference between GSA and MODIS is less than 5% for the desert bright targets. The agreement is slightly worse for urban (it is 8%), shrubland (8.1%) and rain forest (it is 8.9%) sites.

In conclusion, the second release of GSA contains several spatial and temporal extensions and a clear improvement compared with Release 1. The most relevant source of quality-hampering highlighted in the validation of Release 1, i.e. the cloud contamination, has been removed almost entirely. Some known limitations from the previous release remain, but the overall quality of the product is good and Release 2 offer a more reliable data record.

APPENDIX A   DATA RECORD AVAILABILITY

In the following plots, the availability for the 10-day products is presented, together with the data record gaps. The gaps are due to missing input images. As described in the ATBD [AD2] a minimum number of six cloud-free measurements for each day is necessary for the model inversion and albedo retrieval. In the following plots, the gaps for the 10-day period products are shown. Missing products are in red (value 0), while periods where two products are available (from different platform) are plotted in blue (value 2). Green means that one single product is available (value 1).
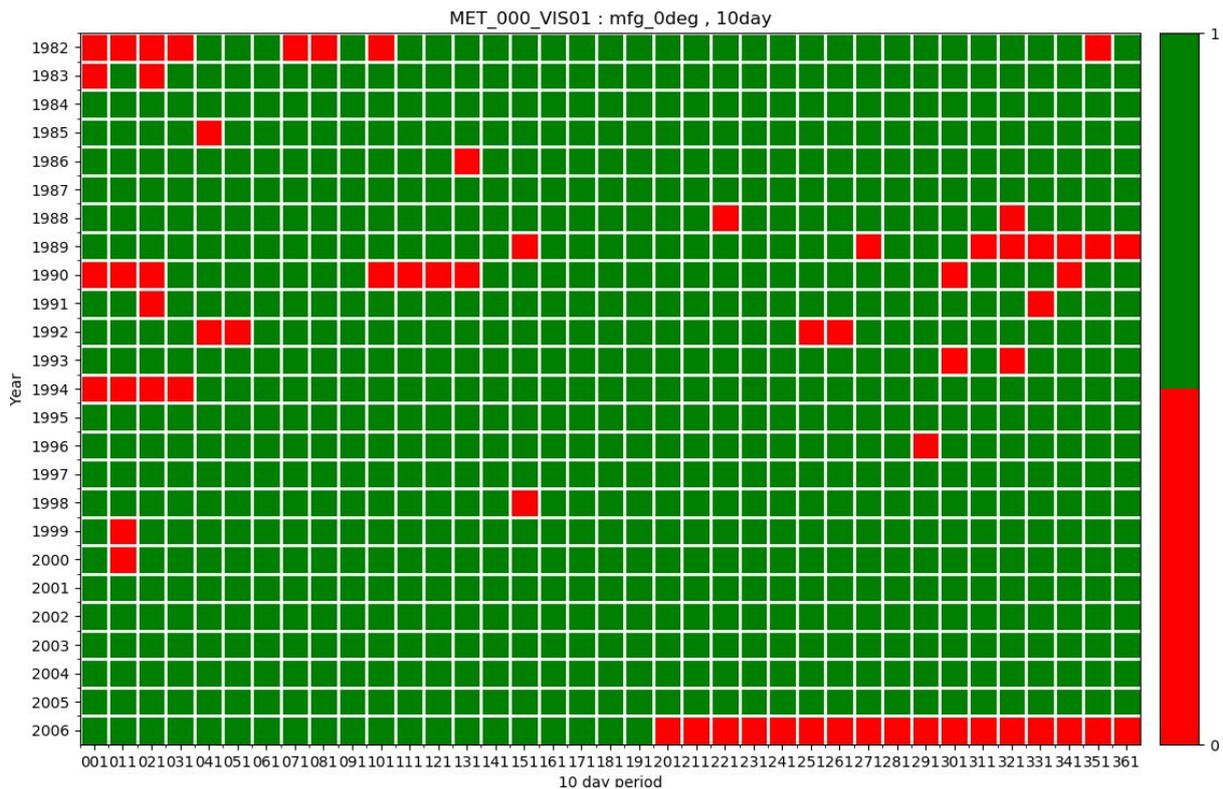

*Figure 32: Gaps for the processing of MFG 0-degree mission.*
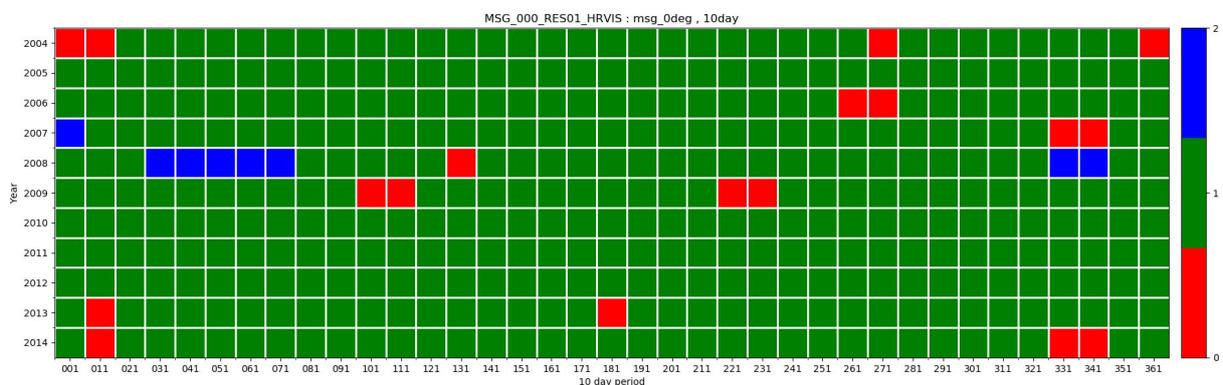
Figure 33: Gaps for the processing of MSG 0-degree mission.
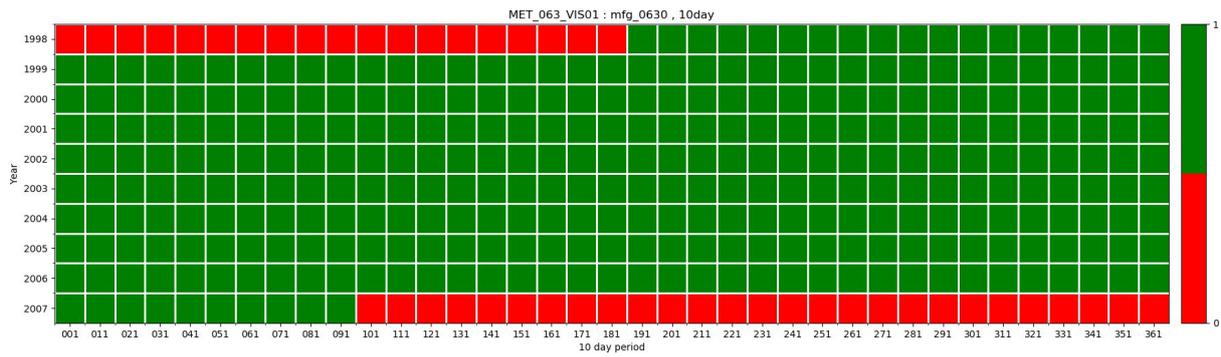
*Figure 34: Gaps for the processing of Meteosat-5 63-degree mission.*
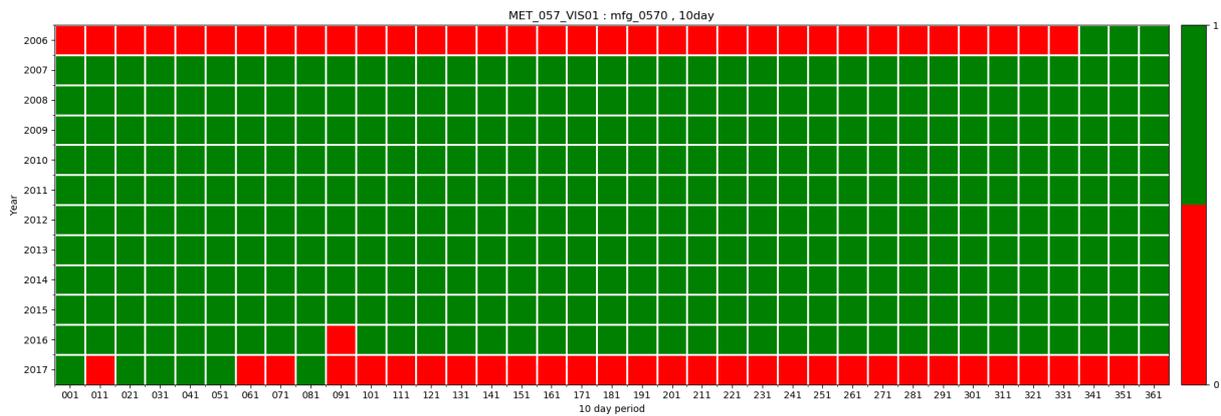
Figure 35: Gaps for the processing of Meteosat-7 57-degree mission.